National Technical University of Athens, NTUA
School of Naval Architecture and Marine Engineering
Shipbuilding Technology Laboratory

Diploma Thesis

Structural Design of Filament Wound Composite Pressure Vessels for Naval Applications

CHATZIPLI Catherine

Thesis Supervisors:
Professor N. TSOUVALIS
Professor N. CARRERE

Athens, March 2023

Acknowledgements

This Diploma thesis was partially carried out at the School of Naval Architecture and Marine Engineering of the National Technical University of Athens (NTUA) - under the supervision of Professor Nicholas Tsouvalis - and at the Institute of Research Dupuy de Lôme (IRDL) at École Nationale Supérieure de Techniques Avancées Bretagne (ENSTA Bretagne) - under the supervision of Professor Nicolas Carrere.

First and foremost, I would like to express the gratitude I feel towards Nicholas Tsouvalis, Professor at NTUA, for giving me the opportunity to work alongside of him and for introducing to me the science of the materials; a topic I have always found very interesting academically. Through his undeniable technical expertise and unconditional support, he meticulously guided this research but most importantly, he affected greatly my thought process as a future engineer.

Secondly, I would like to thank Nicolas Carrere, Professor at ENSTA Bretagne and Georgios Stamoulis, Assistant Professor at UBO, for accepting me in their team at IRDL and for continuously encouraging and supporting me throughout the part of this thesis that has been conducted at ENSTA Bretagne. Their contribution was vital for the completion of this research.

Furthermore, my humble appreciation for the supervision and guidance by Naval Group's team is beyond any explanation. Specifically, Maelle Sergolle, Research Engineer for composite materials and Emilien Bilaudeau, Chief Engineer of R&D projects provided me with not only scientific help of utmost importance, but also engineering experiences I will cherish for the rest of my life.

Moreover, I want to thank my family and my friends for their love and support throughout this research and for fueling me with motivation and pride. They play a significant part in the person and scientist I am slowly but surely becoming.

Last but not least, I would like to thank the person that was by my side for quite literally every single step of the way. During the conduction of this research, Korina Zervou, Naval Architecture and Marine Engineering student was a professional colleague, an academic partner but above all a friend. I am very thankful for her brilliant mind, her continuous help and her very necessary support and that is why I am dedicating this thesis to her.

Abstract

This Diploma thesis is focused on the structural design of composite filament wound pressure vessels and their naval applications. As environmental regulations have been requiring more and more energy saving and eco-friendly material technology, the demand for lighter weight technology of naval applications has caused an increased use of composite materials. Those materials are widely used also for the construction of submersibles, such as pressure vessels, which participate heavily in the naval industry and the most sufficient manufacturing method for such structure is filament winding.

Based on this literature background, this research focuses on the structural design of two case studies of filament wound composite pressure vessels, composed with different geometries, load cases and requirements. These two case studies will be numerically modeled in ABAQUS and tested, using the finite element analysis, in order to optimize their structural characteristics and mechanical behavior. An initial design is given for each case study, accompanied with the material choice of a filament wound composite, geometrical limitations and loads. The purpose of this research is to determine the optimal combination characteristics, so that the two cases will be able to withstand not only linearly but also under nonlinear circumstances. Those characteristics are the material properties, the stacking sequence and the minimum adequate total thickness – hence, the thickness of the plies as well – of the composite tubes. The pressure vessels of those case studies are constructed with flat metal end cups connected to the composite cylinder through an adhesive joint for the first one and with hemispherical composite domes for the second one. Furthermore, the failure criterion chosen for the case studies is the Hashin's Criterion, adapted to Safety Factors derived from the Bureau Veritas Regulations.

For each case study, a parametric analysis is carried out based on its numerical model under linear circumstances, so that it will be clear how much each characteristic of the structure influences the results. After that, if the results indicate that the pressure vessel is likely to fail, the initially proposed characteristics change, with the aim to enhance its ability to withstand the applied load. Finally, a nonlinear analysis is performed, in order to determine whether the model requires to be enhanced even more.

CONTENTS

1. Introduction

1.1 Composite Materials and their Marine Applications

1.1.1 Definition of Composite Materials

From a general point of view, a material that consists of two or more different materials or phases can be considered as a composite one. More specifically, in the science of the materials, the word “composite” is used to describe a material, the elements of which present clear differences from the physics or the mechanics perspective. As a result, their product has significantly different properties in comparison to its components. Those components remain separate inside the composite material, differentiating it from mixtures and alloys.

To be classified in the category of composite materials, the components of said material must agree to the following requirement: the properties of the first component have to be significantly larger than the ones of the rest of the components (≥5 times) and the content by volume of all the components must not be too small (>10%) [Tsouvalis, 1998].

Another definition could be that a material is considered as composite when it consists of two or more chemically distinct components that present a specific separating surface between them. [Agarwal & Broutman, 1990].

One of the parts of a composite material is the reinforcing component and it contributes to the improvement of the mechanical properties of the product. The other one is the matrix, which is usually characterized by a lower density and it ensures that the properties of the reinforcing part are exploited to their maximum potential.

Figure 1.1 shows the combination of three of the main material families (metals, polymers and ceramics) and the resulting composite groups.

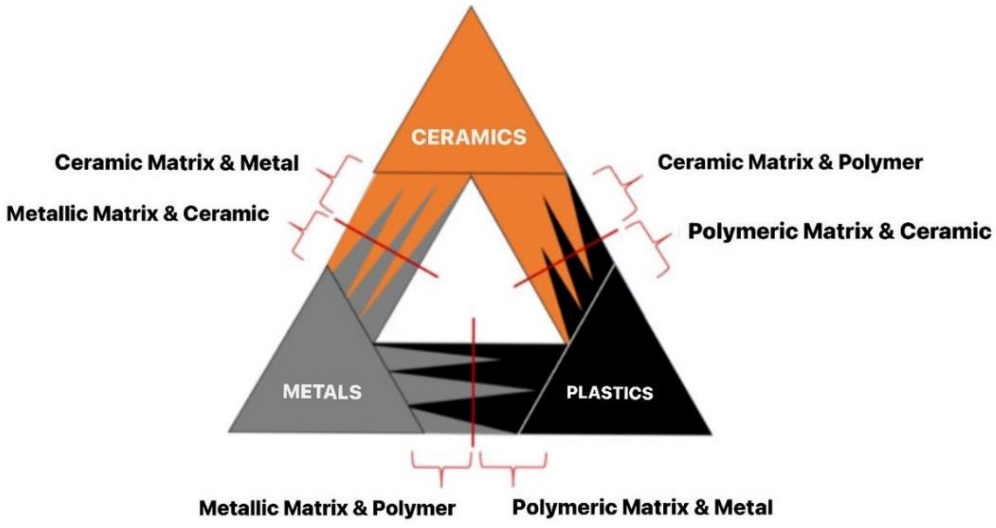

Figure 1.1: Categories of Composite Materials. [Tsouvalis, 1998]

1.1.2 Components of Composite Materials

In the context of this diploma thesis, the composite materials of interest are the ones that use fibers as their reinforcing component. The fibrous composite materials consist of one component called matrix, inside of which are placed fibers of a different material. The term “fibers” refers to reinforcements, which have their one dimension (length) much longer than the others and can be placed either disorderly or with a specific weave and orientation. Due to the alignment of their crystal structure with the axis of their length, it is possible for the fibers to have higher mechanical properties in this direction than any other of the material. The mechanical properties of the reinforcing fibers are the ones that largely determine the properties of the final product. The main strain that can be received by the fibers is the tension in their main direction and therefore, they are immersed in the matrix, which acts as a binding material between them and enables the transfer of the stresses between them and their dispersion at a large range of composite material. In addition, the matrix stabilizes the fibers in a specific position and protects them from environmental damages [Tsouvalis, 1998].

Resins

In order for the matrix to satisfy the needs mentioned above, it should be ductile, durable and relatively flexible. For fibrous composite materials, resins are used as matrix, which are initially in liquid form and through the chemical reaction of polymerization (hardening, curing), they end up taking their solid form. In shipbuilding, organic thermosetting resins are mainly used. The most common types are the polyester, the vinylester, the epoxy and the phenolic ones. The typical properties of the mentioned resins are displayed in Table 1.1. Another category of organic resins are the thermoplastic ones, which soften and can be molded in elevated temperatures.

Table 1.1: Typical Properties of Thermosetting Resins.

Resin	γ $[g/cm^3]$	E [GPa]	v	σ_τ [MPa]	ε_τ [%]	σ_c [MPa]
Polyester (orthophthalic)	1.23	3.2	0.36	65	2	130
Polyester (isophthalic)	1.21	3.6	0.36	60	2.5	130
Vinylester	1.12	3.4	-	83	5	120
Epoxy	1.20	3	0.37	85	5	130
Phenolic	1.15	3	-	50	2	-

In this thesis, the chosen material contains an epoxy resin, so only this type of resins will be analyzed further. Apart from their great adaptability, epoxy resins are known for their high mechanical properties and corrosion resistance. Another advantage of this type of resin is the small shrinkage during the hardening process (1.2 to 4% of their volume), which contributes to excellent bond characteristics when used as adhesives.

Epoxy resins are widely used in multiple industrial sectors: as an adhesive medium in airframe constructions, as interlayer material in the frames of aircrafts, rocket applications and more. They are very useful for sealing, for the manufacture of plastic or metal boats and cars. Also, they are a common choice in electrical applications because of the excellent electrical insulation they offer. For the manufacture of composite materials, they are mainly used in automated production methods such as the filament winding method, which happens to be the chosen method for the production of the pressure vessels of this thesis.

The curing process of epoxy resins requires the addition of a hardener substance and catalyst, in order to control the process, which usually also includes the imposition of high temperatures, between 60ºC and 150ºC. It must be mentioned that there are cold-cure epoxy resins that polymerize at temperatures between 20ºC and 25ºC, but they have lower mechanical properties while also presenting several problems, mainly in terms of viscosity.

Fibers

The reinforcing fibers, as mentioned above, are capable of carrying primarily tensile loads in their principal direction. However, the fibrous composite materials show good mechanical properties in other stresses as well, such as compressive, bending and shear stresses. Their durability is due to the cooperation of the fibers with the resin, where the fibers resist the crack expansion within the resin, while at the same time the resin helps to transfer the stresses to a larger part of the reinforcing fiber, thus reducing its strain. Through this mechanism, a once fragile resin is transformed into a durable composite material, whose properties are higher than those of its components. The majority of shipbuilding applications uses glass fibers, while carbon and aramid fibers are used more and more as well, mainly in high performance structures. Carbon and aramid show noticeably better mechanical properties than the glass ones but their cost is much higher (at least 10 times). Apart from the above, other fibers used to make composite materials are boron, ceramic, as well as various organic fibers, which do not find applications in shipbuilding.

Although the glass fibers are the most common option in the naval industry, in this thesis the chosen material is a carbon fibers, so only this type of fiber will be analyzed further, which are the predominant reinforcement for manufacturing high performance composite materials. Due to the high cost of production, two different categories of carbon fibers are produced: high strength fibers (HS) and the more expensive ones, high modulus fibers (HM), whose typical properties are shown in table 1.2. They are used when an optimum combination of mechanical behavior and weight reduction is required. Their high cost is justified mainly in aerospace applications. Another important feature of theirs is the low expansion coefficient. The carbon fiber production uses polymer fibers of polyacrylonitrile (PAN) as raw material; these are fibers made out of artificial silk (rayon) and tar. Carbon fibers are commercially available in various forms. The basic ones are Chopped Strand Mat (CMT), Rovings and Woven Roving (WR), Woven Fabrics and Unidirectional Rovings (UD). In figure 1.2 the different arrangements of fibers are portrayed.

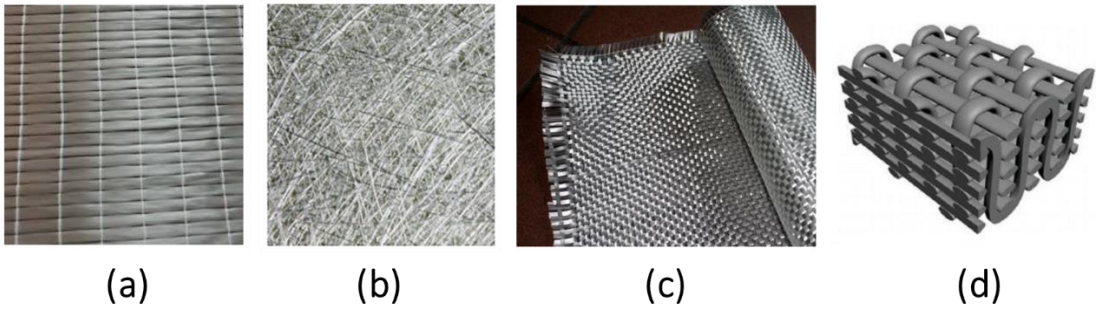

Figure 1.2: Categories of Composite Materials
(a) Unidirectional Rovings (b) Chopped Strand Mat (c) Woven Roving (d) Woven Fabric
[Tsouvalis, 1998].

Table 1.2: Typical Properties of Carbon Fibers.

Carbon Fibers	γ [g/cm^3]	E [GPa]	Carbon Content [%]	σ_τ [MPa]	θ_{max} [ºC]
High Strength(HS)	1.8	180 - 230	95 - 98	2500 - 3400	2000
High Modulus (HM)	1.9	350 - 420	99	1900 - 2300	25000

1.1.3 Naval Applications

The process of introducing and developing structural materials for ship construction is endless. For centuries, wood was the main shipbuilding material until ship builders realized that ships built in iron or steel were stronger, lighter and easier to maintain than those made of wood. During the 1960s composites were widely used in boat building industry in recreational, commercial and military industries. Through the following years, considerable progress has been made on developing the fabrication techniques and on understanding the behavior of these materials and the tailored structures under mechanical, thermal and fire induced load scenarios. Recently, as the IMO's environmental regulations have been strengthened requiring energy saving and eco-friendly material technology, the IMO has also begun to consider operational economics such as energy reduction through lightening the hull. Demand for lighter weight technology using composite materials is increasing. Examples would include lightweight large structures using composite materials, composite materials replacing metal design parts, and polymer composite materials applicable to marine environments.

Different types of composite materials started being an option in naval applications since high performance composites used in yachts such as the ones in the America's Cup or in Route du Rhum races to the less sophisticated applications of glass reinforced fiber-glass used in fishing boats including the applications in naval ships [Chen et al., 2003]. Nowadays, more and more composites are the main materials used for high-speed ships, both catamarans and monohulls. Ship hulls made out of composite materials can usually be regarded as assemblies of a series of stiffened composite panels. Another case used in hulls and structural frames of boats is two layers of carbon fiber reinforced epoxy composites with honeycomb or foam in between them. Marine composite applications include masts and propellers, and other components for recreational or racing sailboats, like the trimaran shown in Figure 1.3. Composite materials can be found in many more areas of a maritime vessel, including interior mouldings and furniture on super yachts.

Figure 1.3: Racing sailboat made of CFRP, participating in Route du Rhum.

The use of composite structure in the integrated superstructure started from naval ships since it reduces the weight and center of gravity of the hull structure but also improves the stability and speed of the ship. Except for the superstructure, naval ships have composite sonar domes, manufactured with vacuum resin transfer molding as presented in Figure 1.4.

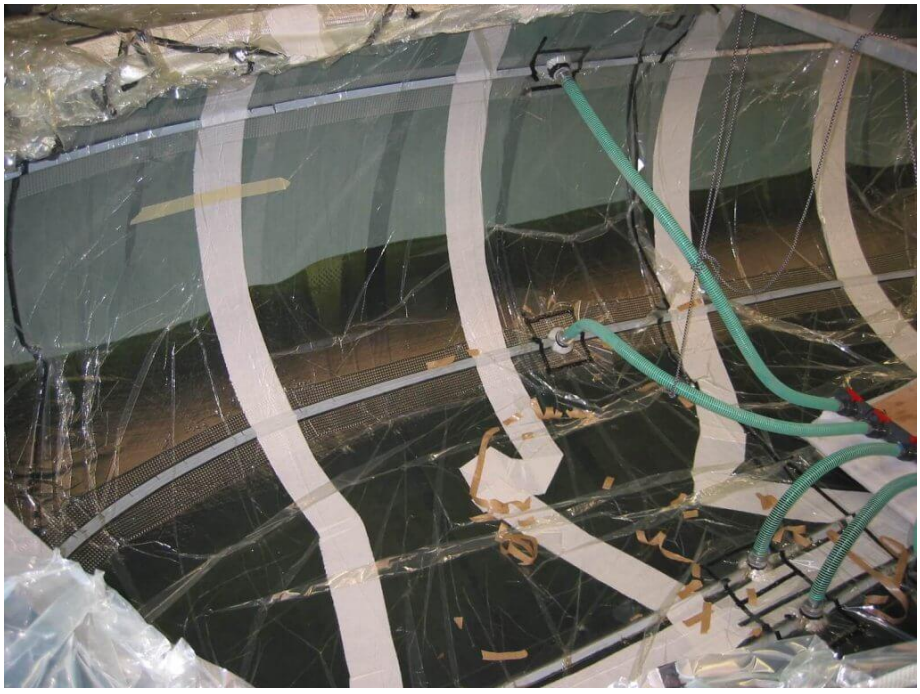

Figure 1.4: Composite sonar under construction [Holland composites].

Furthermore, many traditional rubber parts, which were once used as marine gaskets, are now being made from much stronger composite materials. The same goes for components used in marine engine, propulsion and pump systems including bearings, ducts, shafts, piping, even propellers and rudders. As the marine industry continues to push itself towards more energy-

efficient engines and better preforming parts, the reliance on composites to improve efficiency will keep on growing as well [Rubino et al., 2020].

Composites have been used underwater for many years. The main industries concerned today are offshore oil and gas, oceanography and military. Composite materials are usually chosen in the oil and gas exploration and the production field due to their corrosion resistance and compatibility with the chemicals used downhole and offshore. Razavi Setvati et al. (2014) presents a list of composite applications in offshore marine industry including aqueous piping system, water and fuel storage tanks, low pressure composite valves, floating risers and sub-sea structural components.

The composite materials are widely used also for the construction of submersibles. According to Mouritz et al. (2001), covering the steel hull of a submarine with composite panels is expected to increase the overall buckling strength, lower fatigue strain, reduce corrosion and lower the acoustic, magnetic and electric signatures. Composite materials are also being used in external hull structures in smaller submersibles. Davies (2016) mentions an application for deep ocean exploration called DSV's (Deep Submergence Vehicles). These manned deep sea submersibles [Nautile (France), Shinkai (Japan), MIRs (Russia), Alvin DSVs (USA)], which can reach a depth of 6000 m make use of composites but not for the pressure chamber, which is metallic for all manned vessels. Figure 1.5 shows the Nautile; all the yellow outer fairing is glass reinforced composite but the main pressure vessel housing the crew of three is a titanium alloy sphere.

Figure 1.5: Nautile, the Ifremer 6000m depth manned submersible
[Photo copyright Ifremer/Olivier Dugornay].

According to Davies (2016), composites are also used in the structure of unmanned underwater drones and autonomous underwater vehicles (AUVs). Carbon fiber reinforced composites are used to improve the hydrodynamics of the fairing structure. A more recent application is the pressure resistant housing of profilers, oceanographic instruments which are deployed within the international ARGO project (Figure 1.6). Approximately 4000 robotic instruments, participating in the project, descend to a given depth and then make

measurements of seawater properties (salinity, temperature) while following the ocean currents. They rise to the surface periodically to send the data via satellite, and then re-descend. The name Argo was chosen because the array of floats works in partnership with the Jason earth observing satellites that measure the shape of the ocean surface (https://argo.ucsd.edu/).

Figure 1.6: Oceanographic instrument protection casings (a) Glass/epoxy filament wound housings (500mm long, 150mm inner diameter) (b) Deep Arvor profiler engaged in ARGO project (1000mm long, 100mm inner diameter) [Davies, 2016]

1.2 Pressure Vessels

The AUVs and submersibles mentioned in the previous section could be considered as pressure vessels. More precisely, a pressure vessel is a structures designed to withstand external or internal pressure and it usually takes the form of thin-walled curved shells. This shell-like form is usually more efficient in a spherical shape for such structures because their pressure loading is better withstood in a membrane manner rather than through bending. However, most underwater pressure vessels are shaped differently, given that other shapes serve different but very important purposes apart from structural efficiency.

For instance, a pressure vessel of cylindrical shape would present much higher manoeuvrability underwater than one of a spherical shape. Furthermore, the submarine pressure vessel of cylindrical shape would present fewer difficulties during docking than a spherical one of the same volume. Precise construction of a cylindrical vessel is usually more easily achieved than that of a similar spherical vessel. It must be mentioned, though, that the spherical pressure vessel is useful for miniature submarines and also for deep-diving bathyscaphes [Ross, 2011].

Although a spherical pressure vessel shows great potential for various instances, in this diploma thesis, the cylindrical shape will be analyzed further, given that the case studies examined in chapters 3 and 4 are of such shape.

Most pressure vessel hulls take the form of a cylindrical tube or a cylinder with dome ends, surrounded by a casing, where the purpose of the latter is to improve the hydrodynamic streamlining. However, for a pressure vessel constructed from a combination of cylinders and domes, these structures can fail either through axisymmetric yield or by buckling. The failure due to buckling is shown in Figure 1.7.

Figure 1.7: Shell instability of thin-walled circular cylinders under external pressure. [Ross, 2011]

Very often, the pressure required to cause such shell instability is only a fraction of that necessary to cause axisymmetric yield resulting from a bulk stress. Thus, unstiffened thin-walled circular cylinders are structurally inefficient at withstanding external pressure, particularly if the vessels are wide; one way of improving their structural efficiency is to enhance the structure with ring stiffeners internally, externally, or both. However, for smaller diameters, an unstiffened structure is adequate. Theoretical studies have revealed that internal stiffeners are structurally more efficient than external ones, partly because of their increased curvature and partly because an internal ring-stiffener would weigh less. If, however, the ring stiffeners are not strong enough to prevent structural instability, there is a possibility that the entire pressure vessel could buckle. This form of buckling is called general instability and it is shown in Figure 1.8.

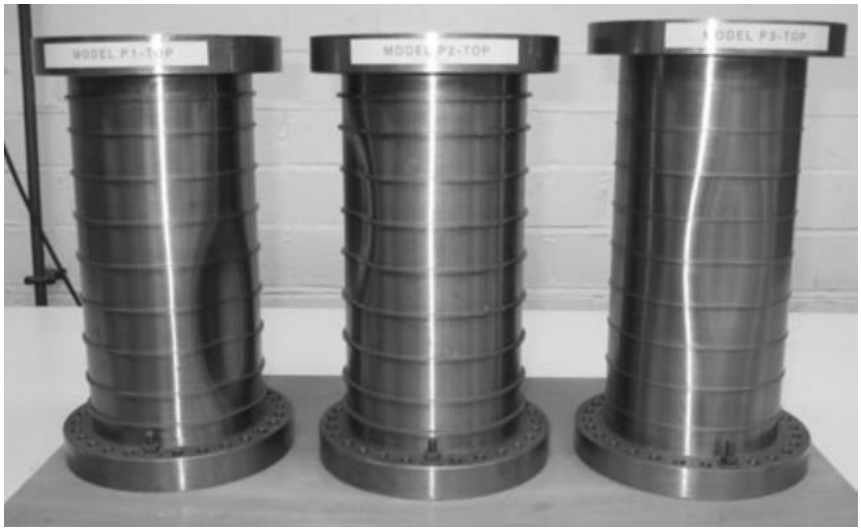

Figure 1.8: General instability of ring-stiffened circular cylinders. [Ross, 2011]

It should be emphasized that owing to initial geometric imperfections the experimentally obtained buckling pressures can very often be considerably lower than predictions based on elastic theory, and therefore it is usually best to design the pressure hull so that buckling is eliminated and any likely failure will be caused by axisymmetric yield. Theoretical estimates of failure pressures based on axisymmetric yield are usually much better than those based on instability, providing the vessel is constructed properly. One question that readers who are not experts in the field may raise is why the ends of a submarine should be blocked off by doubly curved domes instead of flat plates. The reason is, that as flat plates have no meridional curvature, they will have to resist the effects of pressure in flexure and, because of this, in order for them to have equal strength to the circular cylindrical shell to which they are attached, their required thickness may be over ten times that of the circular cylindrical shell.

1.3 Filament Winding Method

For many of the applications mentioned in the previous section, the principal manufacturing method used nowadays is filament winding, which enables composite cylindrical tubes to be manufactured.

In this method, the fiber strands (filaments) are wound continuously on a supportive shape form or mandrel. This method can create axisymmetric items generally in the form of cylinders and tubing, for example, high-pressure containers, tubes and shafts. Filament Winding is an inexpensive and automated method for placing fibers in a precise pattern that adapts to the path of stress by allowing the efficient use of high-strength fibers for enhanced structural efficiency. In other words, the anisotropic fiber properties are optimized. In addition, mass production can cut down the cost further.

Figure 1.8 shows a sketch of a Filament Winding system. A stationary rotating mandrel is used in the Filament Winding process, while a carriage arm moves horizontally with the mandrel. The arm contains a guide or delivery eye which groups and dispenses pre-impregnated fibers called rovings; rovings are usually carbon, Kevlar™, glass fiber, or a hybrid (Azeem et al., 2022). As the mandrel turns, the rovings wrap around it to form a composite winding over the mandrel's surface. The composite winding's exact direction is determined by the carriage rate and the mandrel's rotary velocity. The fibers are impregnated in the resin before they wrap over the mandrel and later solidify with the fiber. After the overwrapping of fiber has been finished, the entire assembly, mandrel plus composite overwrapped layers, is put in the oven to be heated at the required temperatures for curing. The mandrel is removed when the composite resin is fully cured, leaving the hollow composite structure. Nevertheless, optimization of resin type, fiber type, fiber tension, winding thickness, winding angle, and speed, etc., is needed to tailor the product's required final quality.

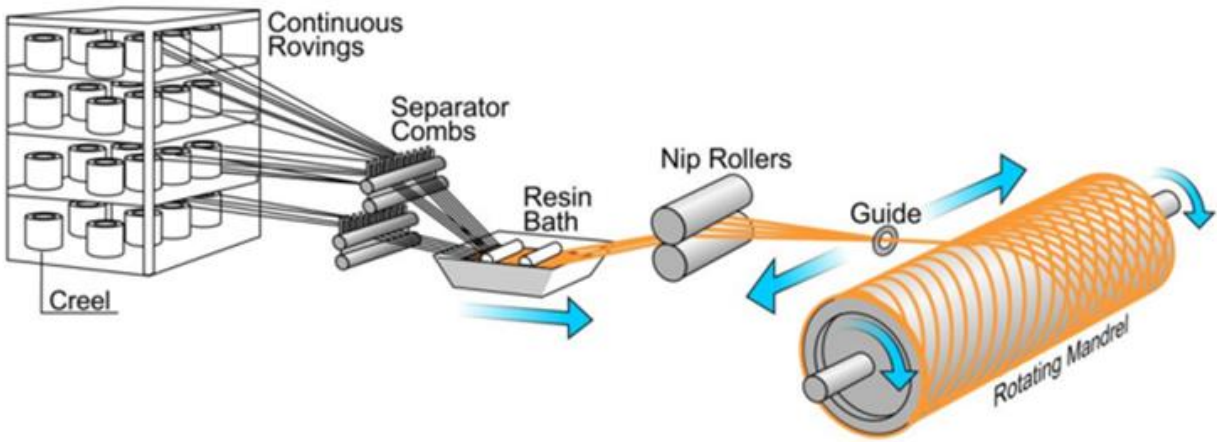

Figure 1.7: Schematics of filament winding process [Tsouvalis, 1998]

There are two typical types of winding machines: helical and polar. In the helical winding machine, the mandrel rotates continuously while the delivery eye moves back and forth. The rotational speed of the mandrel and the linear speed of the delivery eye can be programmed to produce any fiber orientation between 5° and 85°, since filament winding of 0° axial plies or 90° circumferential plies on a tubular structure are not practical in terms of manufacturing feasibility [Peters, 2011]. Several back-and-forth travels of the carriage are needed to complete a lamina covering the mandrel. Such a lamina is always a two-ply balanced laminate at ±θº. In polar winding composite fibers pass tangentially to the polar position and cover the fiber along the polar path, reverses direction, and passes tangentially to the opposite polar position at the other end. In one word, composite fibers are wound from one pole to pole, while the mandrel arm rotates around the longitudinal axis. Polar winders are used to produce spherical vessels or cylindrical vessels with length/diameter ratio less than 2.0. A typical polar winder consists of an arm that rotates around the mandrel delivering the roving into a planar shape. The mandrel is stepped slowly that the arm covers its surface. Except for the perfect sphere, the planar path always has a slip angle with respect to the geodesic path that limits the applicability of polar winding to nearly spherical shapes.

The major limitations of filament winding are size restrictions, geometric possibilities, the orientation of fibers, the surface finish of the final product and residual stresses after curing process. Void content may be high since no vacuum or autoclave is used and the resin cures at low temperature. In Figure 1.8, various filament winders are demonstrated.

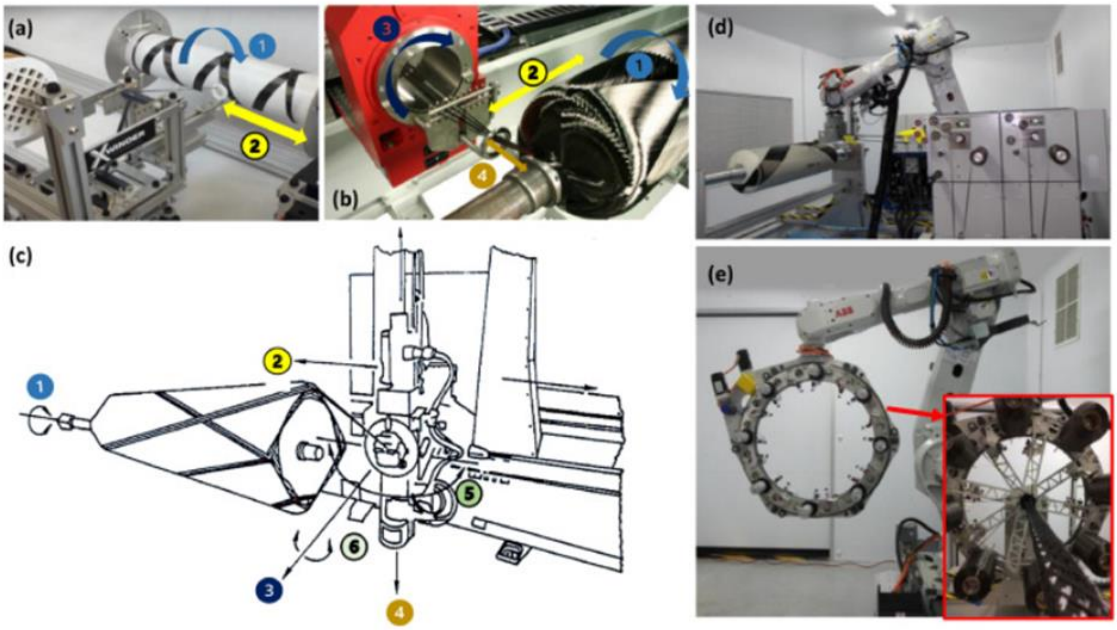

Figure 1.8: (a) 2-axes winder [Xwinder], (b) 4-axes module [MICROSAM], (c) 6-axes winder [McClean Anderson], (d) Robotic winder [Cygnet Texkimp],(e) 3D winder with multiple payout eyes [Cygnet Texkimp]

1.4 Literature Survey and Scope of the Work

1.4.1 Literature Survey

What has been established so far in this thesis is that filament wound composite pressure vessel are widely used in the naval industry for multiple purposes. That is why there are many researchers and experts that have taken it upon themselves to examine a number of cases of said structures under various loading conditions and pressure environments.

In addition, due to the ever-growing use of finite element analysis and numerical modeling, many scientists have conducted studies of comparison between numerical and real experimental results. In this research, for the most part, the load of interest is external pressure. For instance, Moon et al. (2010) has performed experiments and a finite element analysis on moderately thick-walled filament wound carbon–epoxy composite cylinders with metal end cups subjected to hydrostatic pressure. Using the numerical environments of NASTRAN, MARC and ACOS, the buckling pressure of filament-wound composite cylinders was predicted with 2 up to 23% deviation from the test results. Papadakis and Tsouvalis (2016) have carried out a similar research, only they have opted for the ANSYS software. The results this time present a 3 up to 4% deviation from the real experiments. Sulaiman et al. (2013) performed a finite element analysis (FEA) of composite overwrapped pressure vessel (COPV), using commercial software ABAQUS 6.12. The study deals with the simulation of aluminum pressure vessel overwrapping by Carbon/Epoxy fiber reinforced polymer (CFRP). Finite element method (FEM) was utilized to investigate the effects of winding angle on filament-wound pressure vessel. Burst pressure, maximum shell displacement and the optimum winding angle of the composite vessel under pure internal pressure were determined. Tsai-Wu, Tsai-Hill and maximum stress failure criteria were chosen for analyzing data. Results were compared with the experimental ones and there was a good agreement between them.

Another area of interest this diploma thesis focuses on is the parametric study of filament wound composite pressure vessels and the effect certain characteristics of said structures present. This very influence is examined by Tsouvalis, Zafeiratou and Papazoglou (2000). The conclusions stemming from their study provide the valuable information that the performance of the cylinders is greatly affected by its lay-up as expected based on the science of the materials, as well as that the cylinders with flat, rigid end cups are quite stiffer in comparison to the ones with composite hemispherical end domes with respect to buckling, for all thicknesses and stacking sequences examined. Cohen (1997b), on the other hand, was concerned with the influence of filament winding parameters on the quality and strength of composite pressure vessels. He observed that composite strength was significantly affected by the laminate stacking sequence. Geier et al. (2002) agrees with that conclusion, stating that the buckling behavior is definitely influenced by fiber direction and stacking sequence. Another threefold parametric study was carried out by Martins et al. (2014b), who discuss important aspects of the design of composite tubes manufactured by filament winding. This work was divided into the purposes of determining the minimum length that can represent an infinite tube in hydrostatic testing, finding the optimum wind angle of composite tubes subjected to internal pressure under different end conditions and studying the influence of diameter and thickness on the failure pressure during tube burst tests. A progressive failure analysis was performed

using ABAQUS software employing a damage model implemented by a user subroutine (UMAT). The models used were validated using experimental data obtained from tube burst tests in previous studies.

A significant part of this literature survey is the diploma thesis of Tsonos (2017) and the one of Chatzinas (2021). Tsonos' research was focused on CNG storing composite pressure vessels. A simulation model was developed in ABAQUS software, which demanded extensive research concerning the winding trajectories and the thickness build-up at the dome region – this was verified by measuring the thickness of a constructed pressure vessel. This model was used for the conduction of a parametric study, which investigated the design parameters that affect the structural behavior of the pressure vessel and helped in the optimization of its weight. Based on the conclusions of the parametric study, the structural design of a pressure vessel was determined. On the other hand, Chatzinas studied the influencing parameters of the mechanical properties of composite materials, made by filament winding. The specimens examined are mainly ring-shaped, derived from cylinders with different manufacturing parameters such as the type of reinforcement fibers, the geometrical elements, the angle and the winding force of the fibers as well as the used winding twos. The results were subjected to ANOVA statistical analysis, in order to study the effect of the marine environment on the mechanical properties.

1.4.2 Scope of work

This research focuses on the structural design of two case studies of filament wound composite pressure vessels, composed with different geometries, load cases and requirements. These two case studies will be numerically modeled and tested, in order to optimize their structural characteristics and mechanical behavior. An initial design is given for each case study, accompanied with the material choice of a filament wound composite, geometrical limitations and loads. The purpose of this research is to determine the optimal combination characteristics, so that the two cases will be able to withstand not only linearly but also under nonlinear circumstances. Those characteristics are the material properties, the stacking sequence and the minimum adequate total thickness – hence, the thickness of the plies as well – of the composite tubes. The pressure vessels of those case studies are constructed with flat metal end cups connected to the composite cylinder through an adhesive joint for the first one and with hemispherical composite domes for the second one.

2. Problem Description

In order to achieve the purposes of this research, the two case studies will be numerically modelled in way so that they would be as realistic as possible. The finite element environment of ABAQUS is going to be the main tool for numerically modeling the case studies to be examined. Through those numerical models, the effect of various parameters will be examined. Such parameters are the boundary conditions, the number of plies, the material properties, the stacking sequence and the thickness of the structures.

In the next sections of this chapter, the main assumptions for each case study will be established, as well as the failure criterion and the safety factors that will govern them.

2.1 Case Study 1

This first case study concerns a composite filament wound tube sealed with flat metal end cups. These cups are connected to the tube through a metal ring which is bolted to them. There is also an adhesive layer between the end cups and the tube, enhancing the joint. This entire structure is depicted in Figure 2.1 below. Figure 2.1 (a) and (b) present the design of the pressure vessel where the parts with the dots is the composite tube, the stripped (hatched) parts are the metal parts and the grey layer is the adhesive. In Figure 2.1 (c), the metal parts are extracted from the composite cylinder where the grey parts are the metal cups and rings, the red layer is the adhesive and the blue part is the composite cylinder.

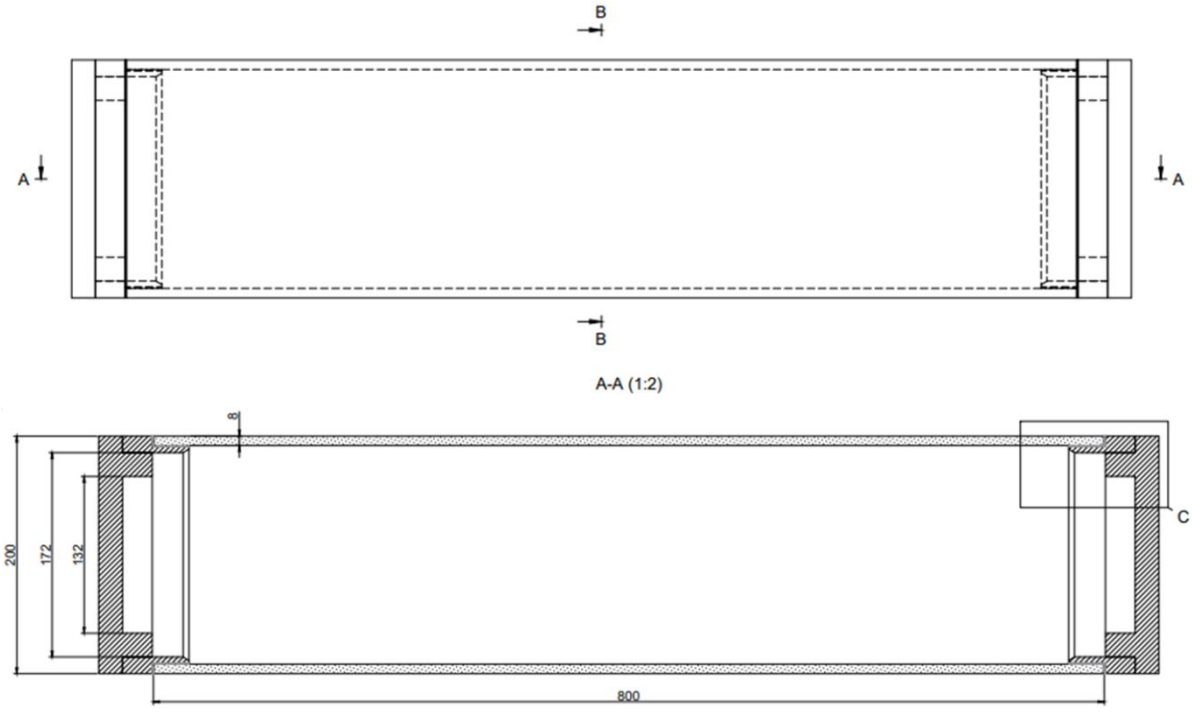

(a)

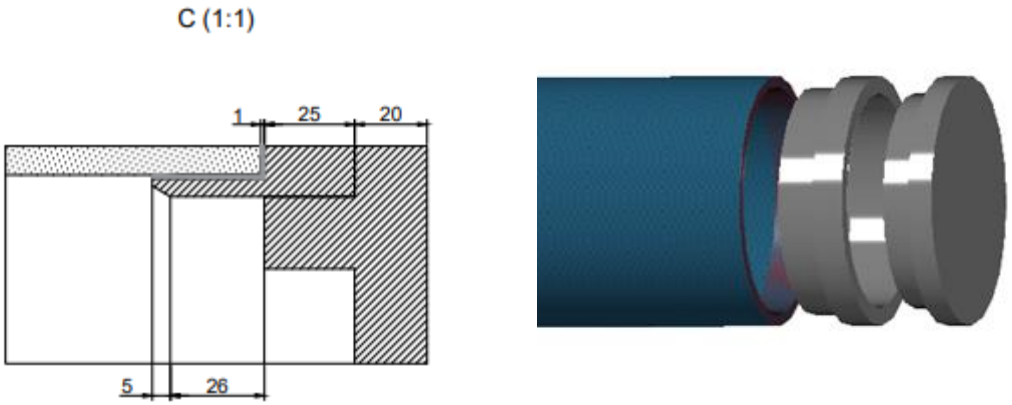

(b) (c)

Figure 2.1: Pressure vessel of Case Study 1 (a) designed (b) zoomed at the joint (c) Extracted model on ABAQUS.

The nominal dimensions of the tube are length 800 mm, internal diameter 184 mm and external one 200 mm, resulting to a nominal thickness of 8 mm. It must be mentioned that the external diameter must remain equal to the nominal one, and cannot be modified. The environment that this structure will have to exist in is under normal circumstances 60 days of salt spray and under exceptional circumstances natural sea water. The temperatures it is meant to encounter under normal circumstances are from -26ºC up to +60ºC and under exceptional circumstances are from -55ºC up to +70ºC. The environmental effects were given at the beginning of the research and they are mentioned for the sake of completeness, however, they were not taken into account eventually. The loading case for this pressure vessel is an external pressure of 4 MPa and an internal one of 0.1 MPa. It is also requested that the material used to fabricate the composite tube of pressure vessel is a CFRP (Carbon Fiber Reinforced Polymer); for the metal end cups and rings, the material is aluminum and the adhesive must be epoxy based. It must be underlined that this diploma thesis is focused only on the composite tube, meaning that the sealing components of this pressure vessel are not modeled at this stage of research.

In this case study, the analyses to be performed are an eigenvalue buckling analysis, a linear static analysis and a nonlinear static analysis considering geometric non-linearities only and taking into account geometric initial imperfections.

2.2 Case Study 2

The second case study concerns a composite filament wound pressure vessel with composite hemispherical dome ends. This structure is depicted more clearly in Figure 2.2 below.

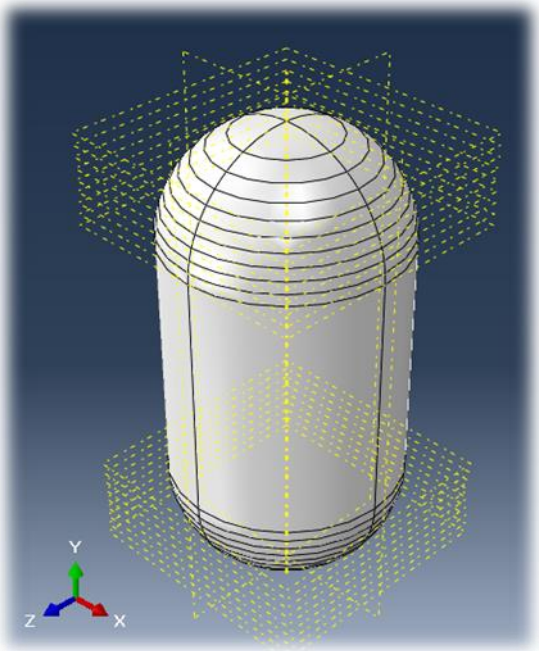

Figure 2.2: Model of Case Study 2 – 500 mm – ABAQUS.

The nominal diameters of the entire vessel are 450 mm internally and 503 mm externally, resulting in a nominal thickness of 26.5 mm. It must be mentioned that the internal diameter must remain equal to the nominal one and cannot be modified. Concerning the cylindrical part of the vessel, the lengths that are considered in this case are various: 500, 1250 and 2000 mm. The environment that this structure will have to exist in (both normally and exceptionally) is natural sea water and the temperatures it is meant to encounter under normal circumstances are from 5ºC up to +70ºC and under exceptional circumstances are from -30ºC up to +70ºC. The same goes for the environmental effects of this case study as for the first one: they were given at the beginning of the research and they are mention for the sake of completeness, but they were not taken into account eventually. The loading cases for this pressure vessel vary as well. Load case 1 is an external pressure of 5 MPa and an internal one of 0.1 MPa. Load case 2 is an external pressure of 0.1 MPa and an internal one of 27.5 MPa. It is also requested that the material used to fabricate this pressure vessel is a CFRP; the same as the one chosen for case study 1.

In this case study, the analyses to be performed are an eigenvalue buckling analysis for load case 1, a linear static analysis assuming geometric non-linearities for the governing load case, which is going to be shown that is load case 1.

2.3 Governing Assumptions

2.3.1 Hashin's Criterion

The failure criterion chosen to be applied to the following numerical analyses is the Hashin's Criterion, which is also the damage initiation criterion for fiber-reinforced composites that ABAQUS uses. This criterion considers four different criteria for damage initiation mechanisms: fiber tension, fiber compression, matrix tension, and matrix compression. Based

on the ABAQUS User's Manual, the damage indicators of the Hashin's Criterion for 2D shell elements, have the following general forms for plane stress conditions:

For fiber tension ($\sigma_{11} \geq 0$):

$$f_f = \left(\frac{\sigma_{11}}{X_T}\right)^2 + \alpha * \left(\frac{\tau_{12}}{S_{12}}\right)^2 \quad (2\text{-}1)$$

For fiber compression ($\sigma_{11} < 0$):

$$f_f = \left(\frac{\sigma_{11}}{X_C}\right)^2 \quad (2\text{-}2)$$

For matrix tension ($\sigma_{22} \geq 0$):

$$f_m = \left(\frac{\sigma_{22}}{Y_T}\right)^2 + \left(\frac{\tau_{12}}{S_{12}}\right)^2 \quad (2\text{-}3)$$

For matrix compression ($\sigma_{22} < 0$):

$$f_m = \left(\frac{\sigma_{22}}{2*S_{23}}\right)^2 + \left[\left(\frac{Y_C}{2*S_{23}}\right)^2 - 1\right] * \frac{\sigma_{22}}{Y_C} + \left(\frac{\tau_{12}}{S_{12}}\right)^2 \quad (2\text{-}4)$$

In equations (2-1)-(2-4):

- $X_{T/C}$: denotes tensile / compressive strength in the fiber direction
- $Y_{T/C}$: denotes tensile / compressive strength in the direction perpendicular to the fibers
- $S_{12/23}$: denotes the longitudinal / transverse shear strength;
- α: is a coefficient that determines the contribution of the shear stress to the fiber tensile initiation criterion. α = 0, if $S_{12} = Y_C/2$. But this is not true for the material properties chosen in this thesis, which means that α = 1.

According to this criterion, if one of the values calculated by the expressions above ends up equal or greater than 1, then failure occurs with the corresponding failure mode.

The equations incorporated in the model with 3D solid elements are derived from ANSYS user's manual, they concern the full 3D stress state and they are the following:

Criticality of tensile loads in the fiber direction ($\sigma_{11} \geq 0$) is predicted with the expression:

$$f_f = \left(\frac{\sigma_{11}}{X_T}\right)^2 + \left(\frac{1}{S_{12}}\right)^2 * (\tau_{12}^2 + \tau_{13}^2) \quad (2\text{-}5)$$

Under compressive loads in the fiber direction ($\sigma_{11} < 0$), failure is predicted with an independent stress condition (for both 2D and 3D):

$$f_f = \left(\frac{\sigma_{11}}{X_C}\right)^2 \quad (2\text{-}6)$$

In the case of tensile transverse stress ($\sigma_{22} + \sigma_{33} \geq 0$), the expression for predicting matrix failure is: ():

$$f_m = \left(\frac{1}{Y_T}\right)^2 * (\sigma_{22}^2 + \sigma_{33}^2) + \left(\frac{1}{S_{23}}\right)^2 * (\tau_{23}^2 + \sigma_{22} * \sigma_{33}) + \left(\frac{1}{S_{12}}\right)^2 * (\tau_{12}^2 + \tau_{13}^2) \quad (2\text{-}7)$$

The following expression is used when the transverse stress is compressive ($\sigma_{22} + \sigma_{33} < 0$):

$$f_m = \frac{1}{Y_C} * \left[\left(\frac{Y_C}{2 * S_{23}}\right)^2 - 1\right](\sigma_{22} + \sigma_{33}) + \left(\frac{1}{2 * S_{23}}\right)^2 (\sigma_{22} + \sigma_{33})^2 + \left(\frac{1}{S_{23}}\right)^2 * (\tau_{23}^2 + \sigma_{22} * \sigma_{33}) + \left(\frac{1}{S_{12}}\right)^2 * (\tau_{12}^2 + \tau_{13}^2) \quad (2\text{-}8)$$

In addition and optionally, the following expression is an out-of-plane version of the Hashin's Criterion that predicts delamination (tension and compression):

$$f_d = \left(\frac{\sigma_{33}}{Z_i}\right)^2 + \left(\frac{\tau_{13}}{S_{13}}\right)^2 + \left(\frac{\tau_{23}}{S_{23}}\right)^2, i = C\ if\ \sigma_{33} < 0, i = T\ if\ else \quad (2\text{-}9)$$

According to this criterion, if one of the values calculated by the expressions above ends up equal or greater than 1, then failure occurs with the corresponding failure mode.

2.3.2 Safety Factor

At this point, it is important to establish the safety factors for the design of both case studies. Based on the Bureau Veritas Regulations [BV NR 546, 2021], each safety factor depends on a series of coefficients related to the ageing effect, the fabrication process and other factors of the material.

More specifically, for Material Failure, the safety factor is defined as:

$$SF = C_{CS} * C_F * C_V * C_i \quad (2\text{-}10)$$

And for the Buckling, the safety factor is defined as:

$$SF_{buck} = C_{buck} * C_F * C_V * C_i \quad (2\text{-}11)$$

In equations (2-10) and (2-11):

- C_{CS} : is the coefficient for combined stresses
- C_{buck} : is the buckling coefficient
- C_F : is the coefficient related to the fabrication process and reproducibility
- C_V : is the coefficient related to the ageing effect of the composite material
- C_i : is the coefficient related to the type of load

In Table 2.1, the values of each coefficient and the characteristic they are respective to are demonstrated. Those values were derived from Bureau Veritas Regulations [BV NR 546, 2021] as well.

Table 2.1: Coefficients for the Safety Factors.

Coefficient	Symbol	Value	Designation
Coefficient related to the ageing effect of the composite material	C_V	1.2	Monolithic Laminate
Coefficient related to the fabrication process and reproducibility	C_F	1.1	Preg, filament winding
Coefficient related to the type of load	C_i	1	-
Coefficient for combined stresses	C_{CS}	1.7	UD, Biaxial, Triaxial
Buckling coefficient	C_{buck}	1.45	-

All in all, after multiplying the values of their respective coefficients, the Safety Factor (SF) for the material ends up equal to 2.24, which means that permissible Hashin's Value – later referred to as SF limit – is equal to:

$$\boldsymbol{SF\ limit = \frac{1}{SF} = 0.45} \quad (2\text{-}12)$$

For buckling, the SF_{buck} ends up equal to 1.91 which also represents the minimum Buckling Factor this study is allowed to result in.

$$\boldsymbol{SF_{buck} = 1.91} \tag{2-13}$$

3. Case Study 1

3.1 Model Description

3.1.1 Geometry

The length of the cylindrical part is equal to 800 mm, the internal diameter is equal to 184 mm and the external one equal to 200 mm, resulting in a nominal thickness of 8 mm.

3.1.2 Material

The type of material for the pressure vessels is CFRP, so the options came down to the type of carbon fibers and resin. The composite material that was proposed initially (CFRP 1) is a carbon fiber reinforced material with 12K type of fibers and an epoxy resin, the properties of which are derived from Tsouvalis, Papadakis and Konstantinidis (2018). The composite material that was finally opted for (CFRP 2) is somewhat different to the first one. It consists of 24K fibers and a bisphenol A type of epoxy, the properties of which are derived from Moon et al. (2010). The main difference between these two composites is that the second one, although it presents more or less the same elastic and shear moduli, it is characterized by higher tensile parallel and perpendicular to the fibers strength and shear strengths. The properties of both CFRP material candidates are presented in Table 3.1 below. Furthermore, the results in this section are calculated based on the material properties of CFRP 1, given that it hasn't yet been proven inadequate for this case study.

Table 3.1: Material Properties of candidate CFRP materials.

		1	**2**	-
CFRP	Fiber	12K T700	24K T700	-
	Matrix	Epoxy	Bisphenol A	-
Elastic modulus	E_1	131.17	121.00	GPa
	E_2	10.86	8.60	GPa
	E_3	10.86	8.60	GPa
Poisson's ratio	ν_{12}	0.280	0.253	-
	ν_{13}	0.280	0.253	-
	ν_{23}	0.382	0.421	-
Shear modulus	G_{12}	4.61	3.35	GPa
	G_{13}	4.61	3.35	GPa
	G_{23}	2.31	2.68	GPa
Tensile strength	X_T	1060.93	2060.00	MPa
	Y_T	26.08	32.00	MPa
	Z_T	26.08	32.00	MPa
Shear strength	S_{12}	9.23	45.00	MPa
	S_{13}	9.23	45.00	MPa
	S_{23}	4.62	64.00	MPa

3.1.3 Stacking Sequence

Due to the fact that the material is a filament wound composite, the stacking sequence will be formed in pairs. The initial stacking sequence studied is 4 pairs of ±55º $[(\pm 55^{\circ})_4]$, adding up to 8 plies, 1 mm thick each. The reason behind choosing the 55º as the initial winding angle is because it is concluded after multiple researches that it is the optimum winding angle for tubes

under external pressure withstanding buckling and by the first ply failure approach of filament wound composite tubes [Tsouvalis et al. (2000), Martins et al. (2014), Almeida et al. (2017)].

Furthermore, the plies of the stacking sequence are layered from the inside to the outside of the cylinder, meaning that Ply 1 is located internally all the way to Ply 8, which is located externally.

3.1.4 Types of Elements & Mesh

This case study has been modeled both with shell and solid elements. The types of elements chosen are S8R, meaning 8-node shell elements with 6 degrees of freedom and reduced integration and C3D20R, meaning 20-node solid quadratic brick elements with reduced integration. The mesh is structured quadratic and the nodes are placed in such a way, so that the elements' aspect ratio is equal to 1, resulting in mostly square shaped elements [Tsouvalis et al., 2000].

More specifically, the initial mesh applied to the cylinder is 20 elements circumferentially and 26 longitudinally, resulting in a total of 520 elements. For the solid elements, there is only one element through the thickness. Figure 3.1 (a) presents the types of elements chosen for the models and (b) and (c) the initial mesh of the model for shell and solid elements respectively.

C3D20R **S8R**

(a)

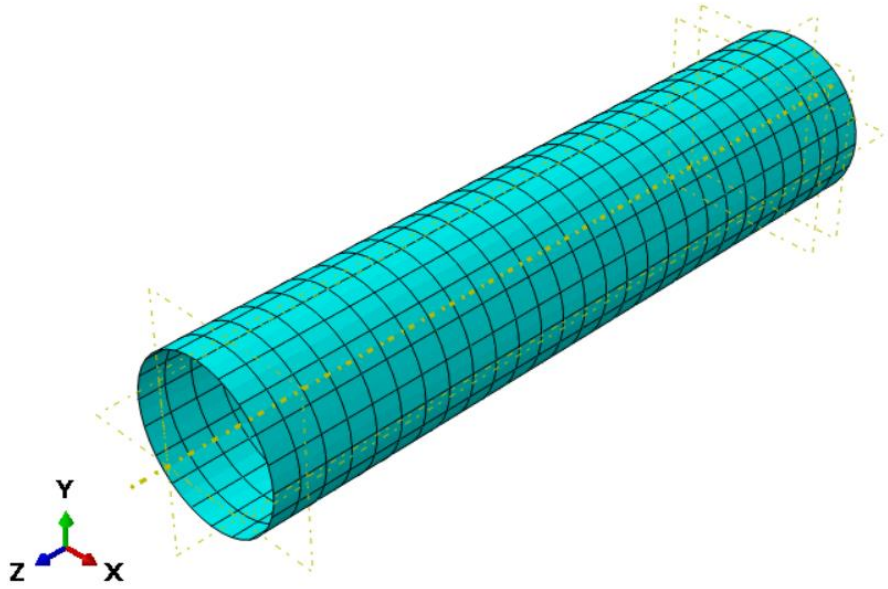

(b)

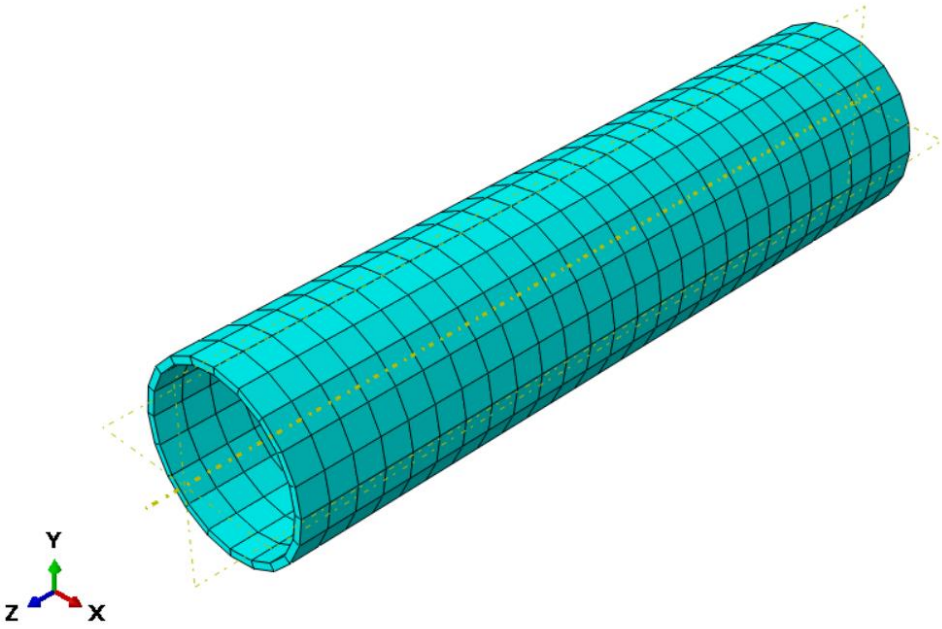

(c)

Figure 3.1: (a) C3D20R & S8R elements used by ABAQUS
Mesh of Case Study 1 for (b) Shell and (c) Solid Elements.

3.1.5 Boundary Conditions & Loads.

The basic boundary conditions set that is proposed is visible in Figures 3.2 and 3.3 for shell and solid elements respectively.

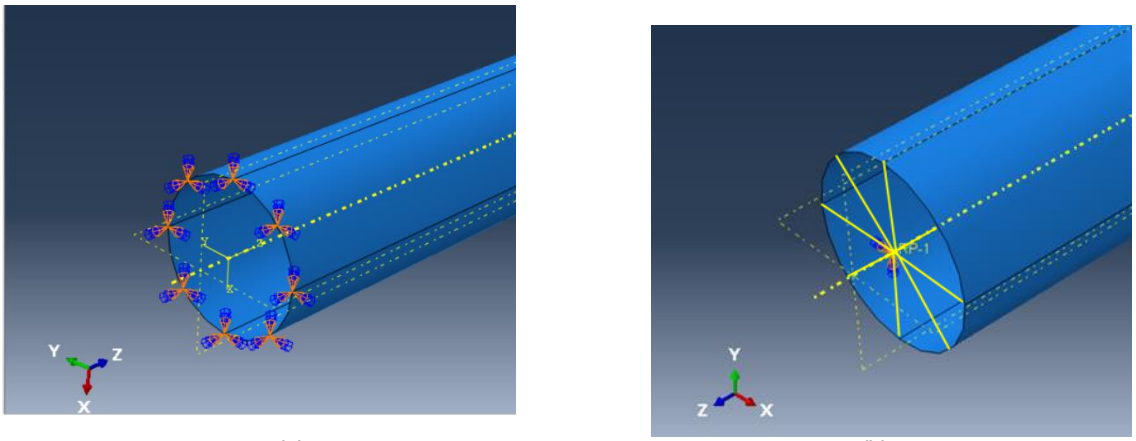

(a) (b)

Figure 3.2: Boundary Conditions for Case Study 1 at (a) End 1 and (b) End 2 – Shell Elements.

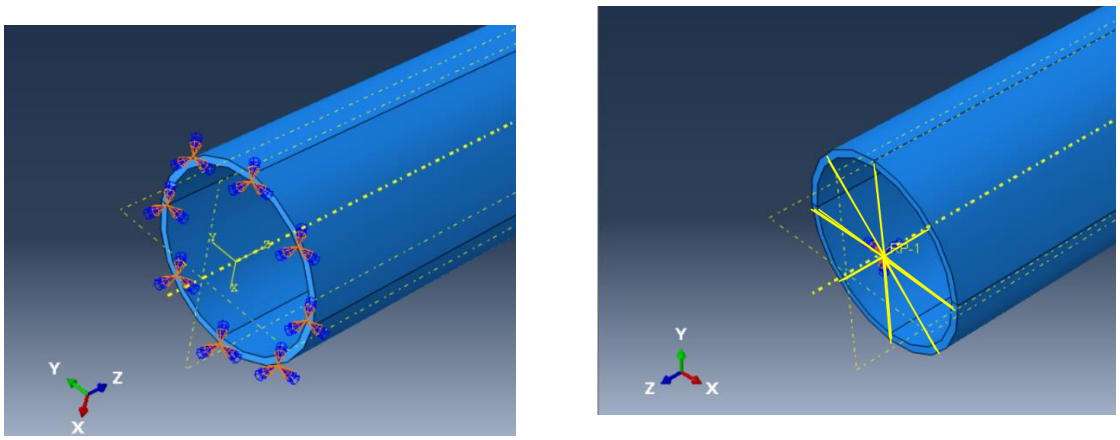

(a) (b)

Figure 3.3: Boundary Conditions for Case Study 1 at (a) End 1 and (b) End 2 – Solid Elements.

For End 1, all degrees of freedom (all translations and rotations) are fixed for all nodes at the circular end of the cylinder. For End 2, a tie constraint (rigid link) is applied linking rigidly all nodes of the circular end to a dummy Master Node located in the center of the circular end. The purpose of this modelling is to represent the metal end cup, which is considered so stiff that it will not be deformed before the composite tube, as the load is applied. All degrees of freedom apart from longitudinal translation of this Master Node are fixed.

The loads applied on this tube are 4 MPa uniform external pressure and 0.1 MPa uniform internal pressure. In addition, a concentrated compressive force is applied to the Master Node in z-direction, representing the load the metal end cup receives. This force is equal to:

$$F = \pi * R_{ext}^2 * P_{ext} - \pi * R_{int}^2 * P_{int} = 123005\ N$$

This basic boundary conditions set will be examined in the chapter of the parametric study.

3.1.6 Initial Results

Eigenvalue Buckling

Based on the model with the assumptions mentioned in the above sections, an eigenvalue buckling analysis has been carried out, resulting in the following first 10 eigenvalues (Table 3.2) and in their respective modeshapes (Figure 3.4 (a)-(j)).

Table 3.2: Initial Results – Eigenvalue Buckling.

Eigenvalue number	Value	Buckling Modeshape	Figure
1	3.045	2.1	(a)
2	3.045	2.1	(b)
3	6.720	2.2	(c)
4	6.720	2.2	(d)
5	6.770	3.1	(e)
6	6.770	3.1	(f)
7	7.553	2.3	(g)
8	7.553	2.3	(h)
9	9.102	3.3	(i)
10	9.102	3.3	(j)

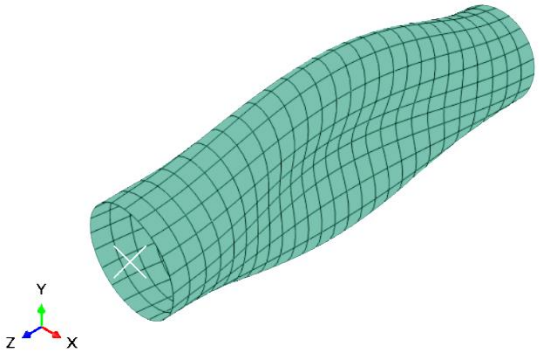

(a)

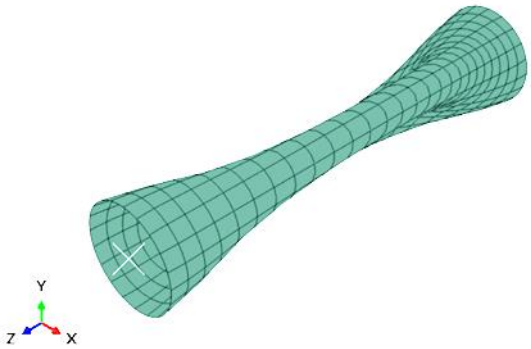

(b)

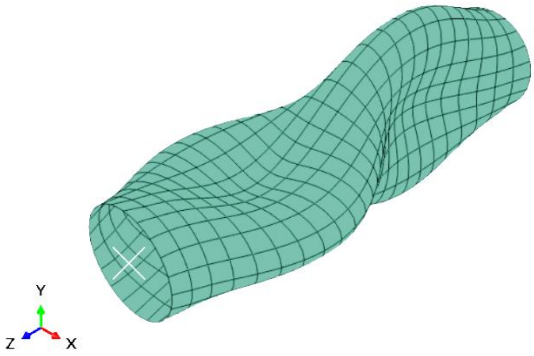

(c)

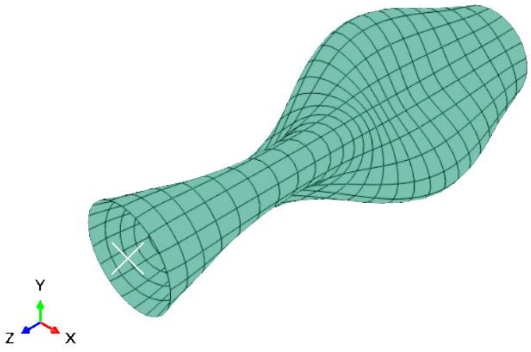

(d)

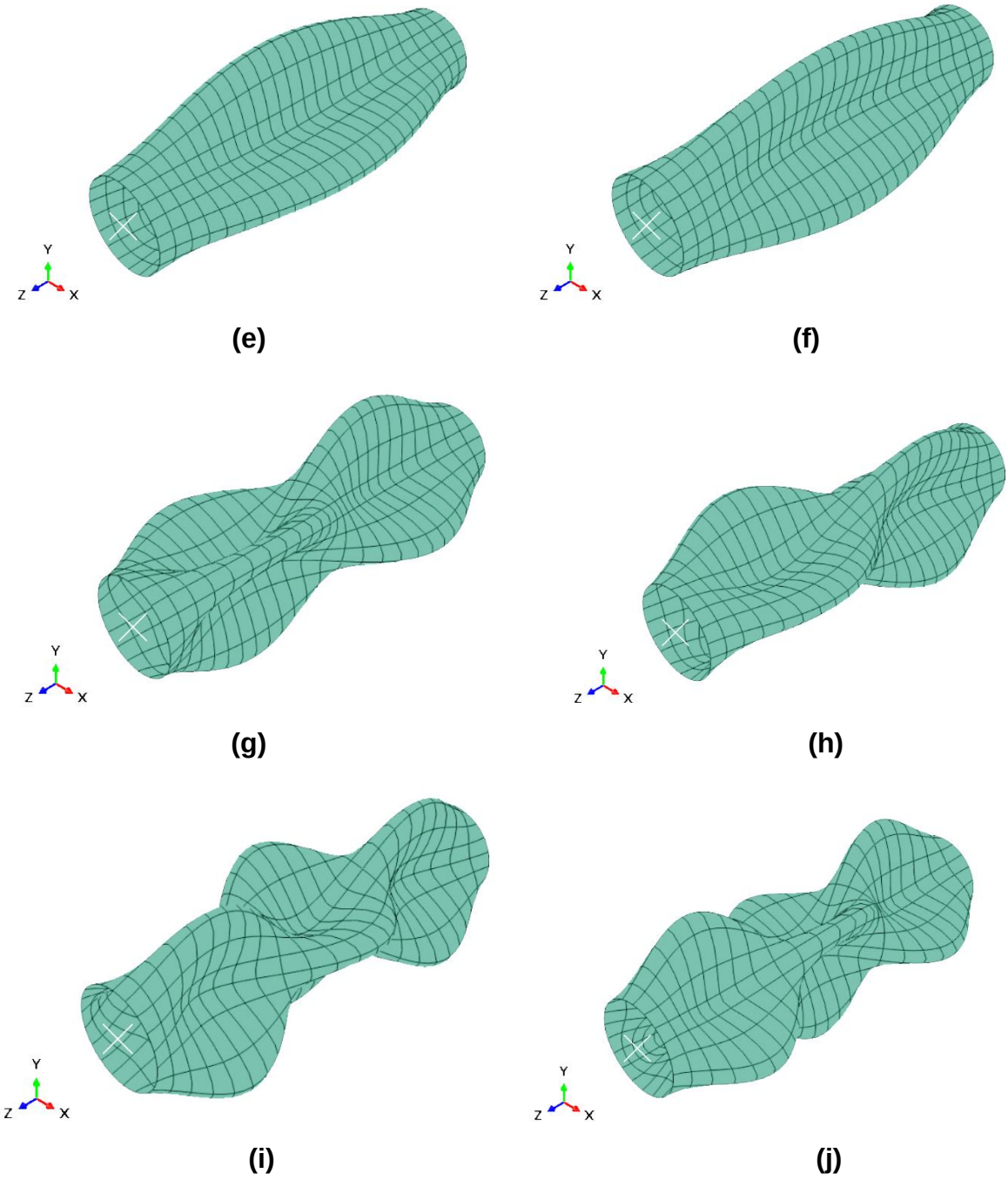

Figure 3.4: Modeshapes of each eigenvalue – Case Study 1.

Linear Static Analysis

Apart from eigenvalue buckling analysis, a linear static analysis has been carried out as well, resulting in the following fiber and matrix values calculated by equations (2-1)-(2-4) the Hashin's Criterion (Table 3.3) and in the deformed shape is depicted in Figure 3.5.

Table 3.3: Initial Results – Linear Static Analysis.

For Ply 1 – At the circular end	Symbol	Value
Hashin's Criterion - Fiber Compression	f_f	0.0043
Hashin's Criterion - Matrix Compression	f_m	0.3258
Stresses [MPa]	S_{11}	-69.8296
	S_{22}	-12.7480
	S_{33}	0.0000
	S_{12}	6.5092

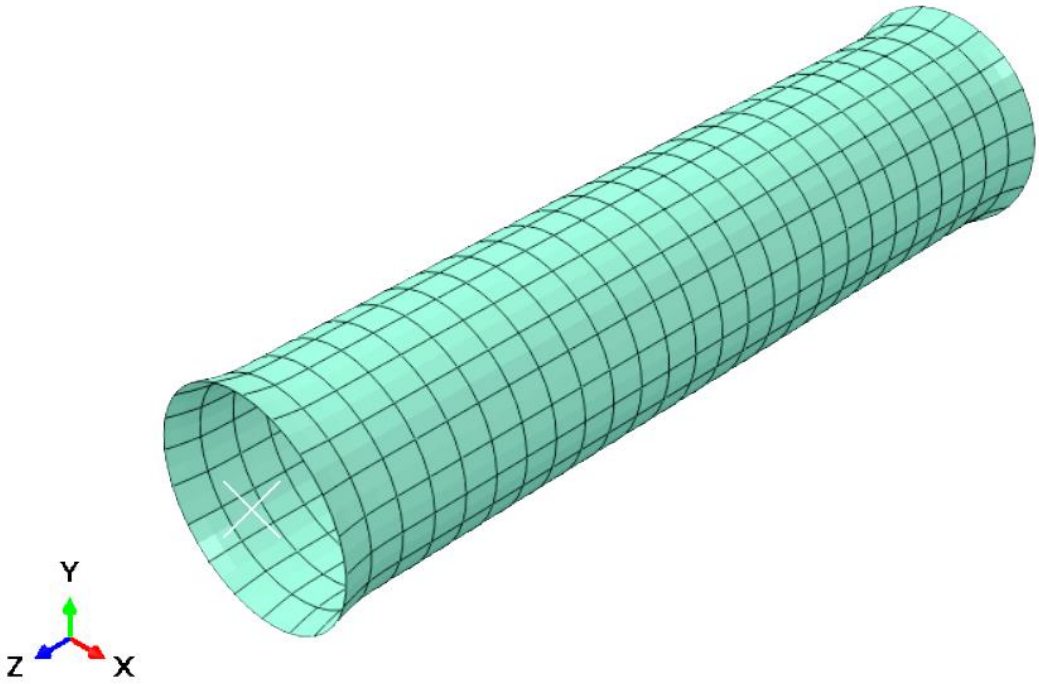

Figure 3.5: Deformed shape after the linear static analysis – Case Study 1.

3.2 Parametric Study

This investigation began with a parametric study based on eigenvalue buckling analysis results, in order to start settling on the final characteristics of the composite tube. The goal is to model the structure in the most realistic way that is possible and to optimize its stacking sequence in order to reach an as small as possible thickness value (and hence weight of the structure) that can safely withstand the required loading, taking additionally into account the required safety factor.
The parameters examined within this parametric study are:

1. Mesh size
2. Number of Plies
3. Stacking Sequence
4. Boundary Conditions

In order to see also how important some of the problem parameters are, a sensitivity analysis was carried out investigating the effect of:

a. Cylinder Thickness

b. Material Properties
c. Ovalization of the Tube

The parametric study was done based on the shell elements model, due to the fact that the solid elements model is more resources demanding.

3.2.1 Mesh Convergence Study

The first step of the parametric study concerns the mesh magnitude of the model. The parameters that remain constant for this study are explained in Table 3.4.

Table 3.4: Constant Parameters – Mesh Convergence Study.

Total Thickness [mm]	t_{tolal}	8
Ply thickness [mm]	t	1
Total plies	n	8
Element Type	S8R	8-node doubly curved thick shell, reduced integration - Structured Quadratic - 6 DOFs
Boundary Conditions	End 1	Fully fixed – All DOFs of all its nodes.
	End 2	Only the Longitudinal Translation is free.
CFRP	1	Reference Table 3.1
Stacking Sequence	-	$(\pm 55^{o})_4$

The final mesh to be chosen must be the least fine, so that the computational time will be as short as possible but without influencing the accuracy of the results. Table 3.5 demonstrates the various number of elements examined and the results produced by them. The second column of the table presents the mesh magnitude – the first number is the number of elements circumferentially and the second one is the number of elements longitudinally. The third column is the external pressure that, if applied on the pressure vessel, buckling will occur and in the modeshape respective to the eigenvalue calculated, which is noted in the last column of the table. The eigenvalue this research focuses on is always the first one. The fourth column is the aspect ratio, which needs to be almost equal to 1 so that the elements have a shape as close to square as possible. Finally, the fifth column shows the difference of the results each mesh produces in comparison to the least fine mesh, in order to determine whether the model is converged when the least fine mesh is applied. Moreover, Figure 3.6 depicts those results in a form of a diagram.

Table 3.5: Mesh Convergence Study – Results – Case 1.

Number of Elements	Meshing	External Buckling Pressure [MPa]	Aspect Ratio	Difference to the least fine mesh [%]	Buckling Modeshape
520	20x26	11.9008	1.021	0.000	2.1
1584	36x44	11.8976	0.959	0.000	2.1
2000	40x50	11.8972	0.981	0.027	2.1
2976	48x62	11.8972	1.014	0.033	2.1
3432	52x66	11.8972	0.996	0.033	2.1

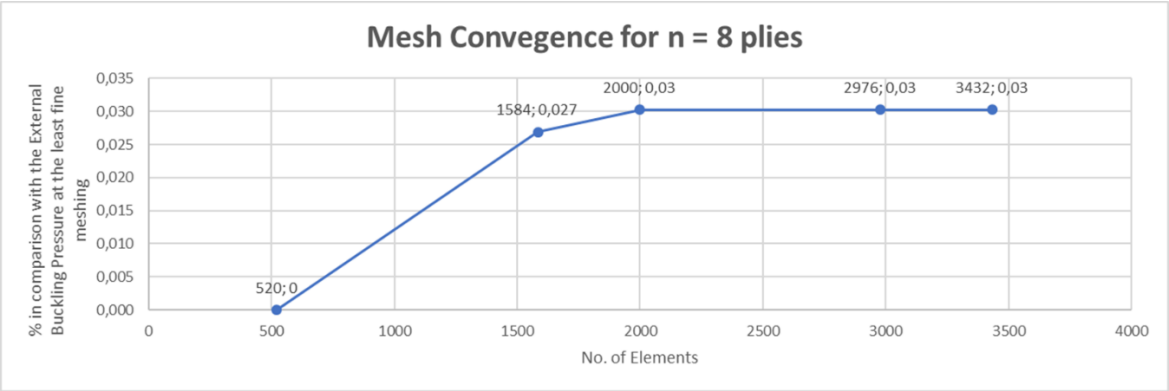

Figure 3.6: Diagram of the Mesh Convergence Study – Case 1.

Based on the above results, it is obvious, not to mention comforting, that the model was more or less converged from the beginning. Keeping the lowest number of elements as a reference point, it seems that the percentage of difference between the results doesn't exceed the 0.03% even when the number of elements is practically 7 times higher than the initial one. This means that a total of 520 elements – 20 circumferentially and 26 longitudinally with an aspect ratio of 1.021 – are a safe choice for this model.

3.2.2 Number of Plies Effect

In this section, the number of plies that the material will be modeled with is determined. The parameters that remain constant for this study are explained in Table 3.6.

Table 3.6: Constant Parameters – Number of Plies Effect.

Total Thickness [mm]	t_{tolal}	8
Ply thickness [mm]	t	1
Element Type	S8R	8-node doubly curved thick shell, reduced integration - Structured Quadratic - 6 DOFs
Mesh	-	20 elements circumferentially and 26 longitudinally – 520 elements total
Boundary Conditions	End 1	Fully fixed – All DOFs of all its nodes.
	End 2	Only the Longitudinal Translation is free.
CFRP	1	Reference Table 3.1
Stacking Sequence	-	$(\pm 55^{o})_4$

The reference case is that with 8 plies. Table 3.7 demonstrates the various number of plies examined as well as the thickness of each ply and the results produced by them. The third column is the external pressure that, if applied on the pressure vessel, buckling will occur and in the modeshape respective to the eigenvalue calculated, which is noted in the last column of the table. The fourth column shows the difference of the results each number of plies produces in comparison to the originally proposed one, which is 8 plies, in order to determine whether the model is converged when the initially proposed amount of plies is modeled. Moreover, Figure 3.7 depicts those results in a form of a diagram and as it is clear from it, the convergence is attained after the case of 20 plies.

Table 3.7: Number of Plies Effect– Results – Case 1.

Ply Thickness [mm]	Number of Plies	External Buckling Pressure [MPa]	Difference to the 8-ply material [%]	Buckling Modeshape
0.1	80	12.27	3.14	2.1
0.2	40	12.26	3.05	2.1
0.4	20	12.22	2.67	2.1
0.5	16	12.18	2.38	2.1
0.8	10	12.04	1.14	2.1
1	8	11.90	0.00	2.1

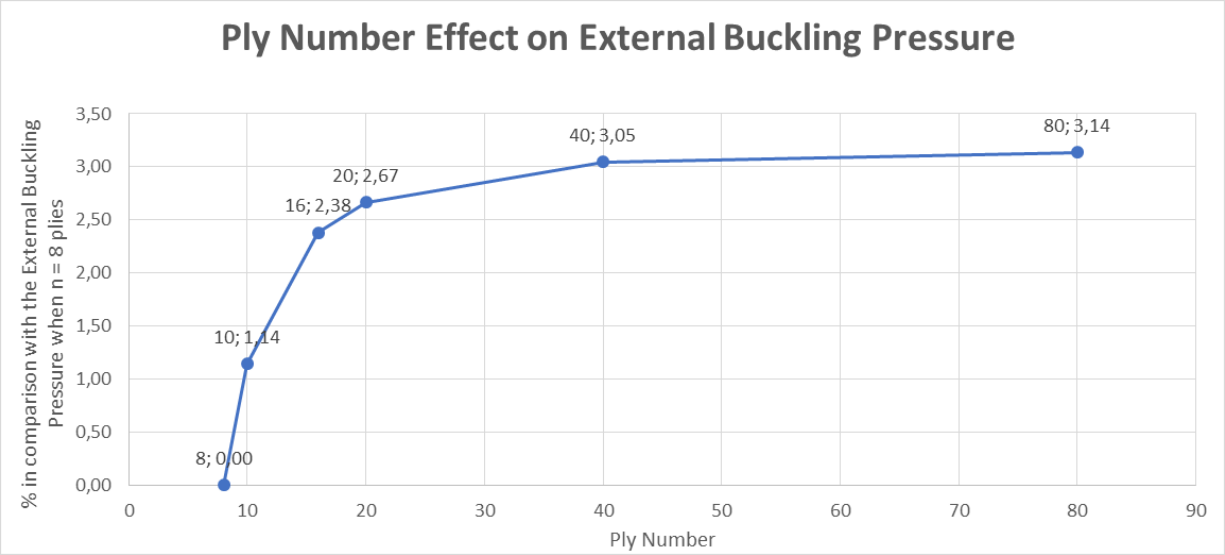

Figure 3.7: Diagram of the Number of Plies Effect – Case 1.

Keeping in mind that the simplest model possible is the desirable one, the 20-ply material fulfils this purpose without affecting the accuracy of the results. Another information provided at this point is that the thickness of the ply will be 0.4 mm given that the nominal total thickness is equal to 8 mm.

The results from this point forward are based on the model with a 20-ply composite material.

3.2.3 Stacking Sequence Effect

This next part examines the stacking sequence effect on the buckling behavior of the tube. The parameters that remain constant for this study are explained in Table 3.8.

Table 3.8: Constant Parameters – Stacking Sequence Effect.

Total Thickness [mm]	t_{tolal}	8
Ply thickness [mm]	t	1
Number of Plies	n	20
Element Type	S8R	8-node doubly curved thick shell, reduced integration - Structured Quadratic - 6 DOFs
Mesh	-	20 elements circumferentially and 26 longitudinally – 520 elements total
Boundary Conditions	End 1	Fully fixed – All DOFs of all its nodes.
	End 2	Only the Longitudinal Translation is free.
CFRP	1	Reference Table 3.1

Table 3.9 demonstrates the various stacking sequences examined and the results produced. It is interesting to note that the modeshape is different for the stacking sequence of $[\pm 30^{o}]_{10}$. Moreover, Figure 3.8 depicts those results in the form of a diagram.

Table 3.9: Stacking Sequence Effect– Results – Case 1.

Stacking Sequence [±θº]	External Buckling Pressure [MPa]	Buckling Modeshape
30	8.80	3.1
45	10.02	2.1
55	12.22	2.1
60	13.70	2.1
65	15.23	2.1
70	16.66	2.1
75	17.88	2.1
80	18.78	2.1
90	19.49	2.1

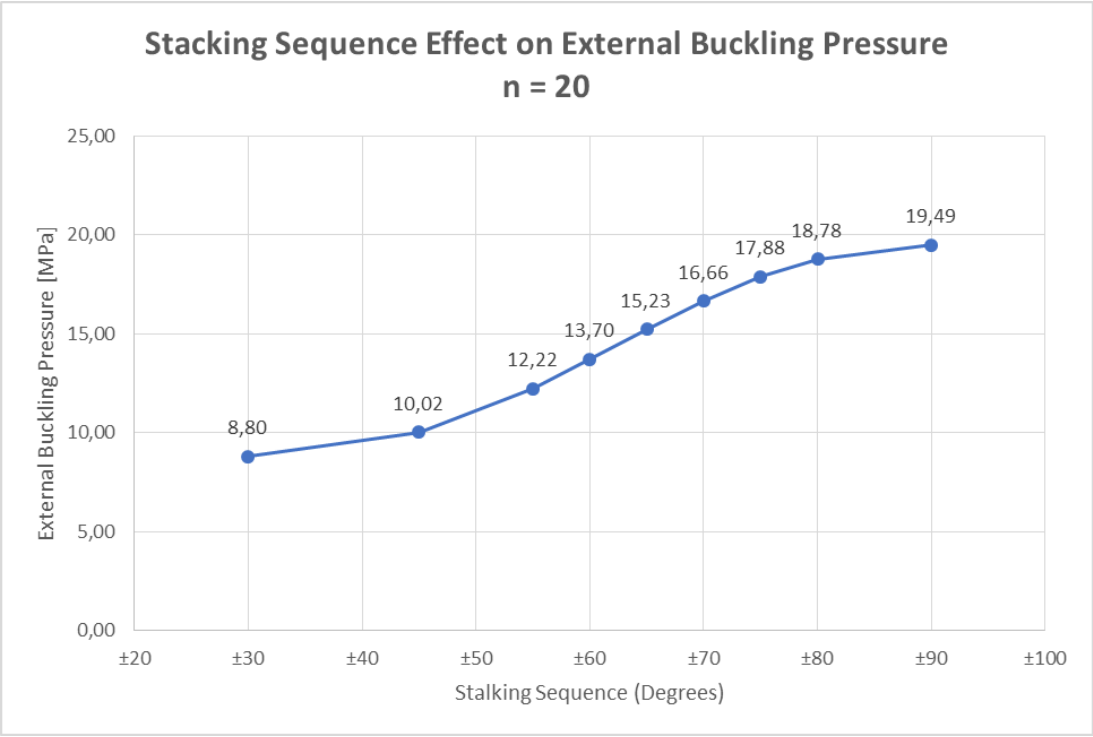

Figure 3.8: Diagram of the Stacking Sequence Effect – Case 1.

In an imaginary circumstance where the only phenomenon influencing the pressure vessel is buckling, the optimum $[\pm \theta^{o}]$ stacking sequence would be $[\pm 90^{o}]_{10}$, which results in the highest buckling factor in comparison with the rest of the stacking sequences. And that is something expected, given that buckling under external pressure requires high stiffness in the circumferential direction of the cylinder.

However, what must be taken into consideration is the possibility of resulting in failure because of the material. Redirecting the attention to that and putting to use the Hashin's Criterion for compression, the values in Table 3.10 and the diagram in Figure 3.9 are produced and make it clear that the options for the optimum stacking sequence are much more limited. Table 3.10 shows present the Hashin's Criterion values for fiber and matrix respectively, as well as the part of the plies that this value characterizes.

Table 3.10: Hashin's criterion results for various ±θ Stacking sequences – Case 1

Hashin's Criterion (max) - Compression						
# of Stacking Sequence	Stacking Sequence [±θº]	Fiber	Ply	Matrix	Ply	Failure
1	30	0.02	inner	4.500	outer	YES
2	45	0.009	inner	1.120	inner	YES
3	55	0.004	outer	0.313	inner	-
4	60	0.004	outer	0.530	inner	-
5	65	0.003	outer	0.815	inner	-
6	70	0.003	outer	1.177	inner	YES
7	75	0.004	outer	1.456	inner	YES
8	80	0.002	outer	1.667	inner	YES
9	90	0.002	outer	1.749	inner	YES

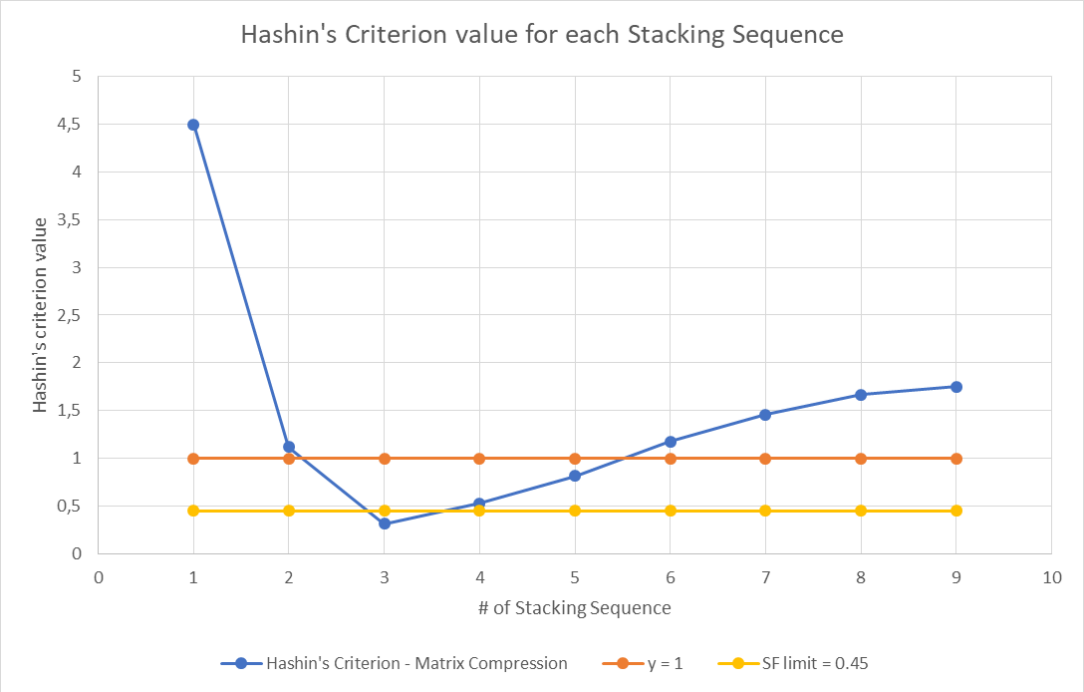

Figure 3.9: Diagram of the Hashin's Criterion – Case 1.

As one can easily predict, the higher Hashin's Criterion value match the Matrix. From Figure 3.9, it seems that the winding angles that do not fail based on the Criterion, are the 55, 60 and 65º. Furthermore, the only one that does not fail even when the Safety Factor is considered, is the 55º.

So, finally, the proposed stacking sequence is $[\pm 55^{\circ}]_{10}$ and that is the one which the tube will be modeled with from now on.

3.2.4 Effect of Boundary Conditions

At this point, the boundary conditions are up for investigation. The parameters that remain constant for this study are explained in Table 3.11.

Table 3.11: Constant Parameters – Stacking Sequence Effect.

Total Thickness [mm]	t_{tolal}	8
Ply thickness [mm]	t	1
Number of Plies	n	20
Element Type	S8R	8-node doubly curved thick shell, reduced integration - Structured Quadratic - 6 DOFs
Mesh	-	20 elements circumferentially and 26 longitudinally – 520 elements total
CFRP	1	Reference Table 3.1
Stacking Sequence	-	$(\pm 55^{o})_{10}$

This subject has been a principal question during this parametric study. In general, the boundary conditions is very difficult to be 100% realistic but they should provide certain characteristics to the model, so that its structural behaviour and deformed shape be as close to reality as possible. Speaking of which, the deformation is expected to be symmetrical, given the nature of this case study. It may also result in the loss of the planar shape of the circular ends, but this depends on the stiffness of the cup. It is beneficial to have stiffer cups and to not lose the planar shape of the ends because, in that way, the buckling factor ends up higher. That is why in Table 3.12, which presents all the different boundary conditions cases investigated along with their corresponding results, only the sets of boundary conditions that provide such results are shown. The term DOF means Degrees Of Freedom and Figure 3.10 depicts a typical (2.1) modeshape.

Table 3.12: Candidate Sets of Boundary Conditions – Case 1

# of set	End 1	End 2	Axial Loading	External Buckling Pressure [MPa]	Difference to set 1 [%]
1	Fully fixed – All DOFs of all its nodes are fixed.	Master Node - Transvers translations and all rotations are fixed.	Axial Force at End 2	12.22	0.00
2		Master Node - All DOFs are free.	Axial Force at End 2	12.24	0.20

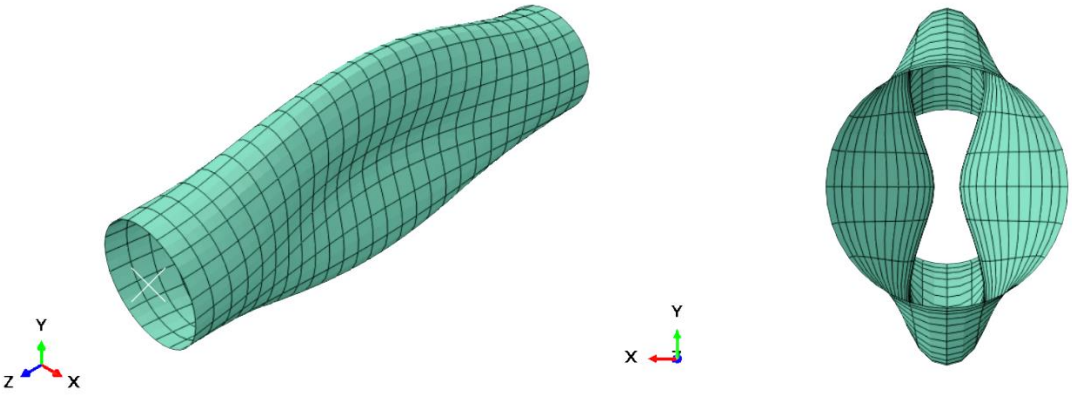

(a) (b)

Figure 3.10: Deformation resulting from the examined Boundary Conditions – Modeshape 2.1.

As it is clear from Table 3.12, the differences are negligible, not exceeding 1%. This means that as the boundary conditions change, the buckling factor will not be substantially affected.

All in all, the boundary conditions of the model remain the same as the ones of the initial assumptions: For End 1, all degrees of freedom are fixed for all the nodes around the circular end of the cylinder. For End 2, a tie constraint is applied linking rigidly the elements of the circular end to a Master Node in the center with all its degrees of freedom apart from the longitudinal translation fixed.

3.2.5 Sensitivity Analysis

Unfortunately, in reality, any structure's nominal characteristics, such as its total thickness or the properties of the material are never exactly equal to the actual ones. These two characteristics are examined in the following sensitivity analysis. The objective is to observe how severe their effect is on the results.

Total Thickness

The parameters that remain constant for this study are explained in Table 3.13

Table 3.13: Constant Parameters – Stacking Sequence Effect.

Total Thickness [mm]	t_{tolal}	8
Ply thickness [mm]	t	1
Number of Plies	n	20
Element Type	S8R	8-node doubly curved thick shell, reduced integration - Structured Quadratic - 6 DOFs
Mesh	-	20 elements circumferentially and 26 longitudinally – 520 elements total
Boundary Conditions	End 1	Fully fixed – All DOFs of all its nodes.
	End 2	Only the Longitudinal Translation is free.
Stacking Sequence	-	$(\pm 55^{o})_{10}$
CFRP	1	Reference Table 3.1

Table 3.14 presents the results for the total thickness sensitivity analysis. The total thickness has been reduced and increased by 5 and 10%. This procedure was performed for nominal thicknesses of 6, 8 and 10 mm, just to obtain a more general glimpse of the structure's behavior when it comes to its thickness variation. Keeping the nominal thickness as a reference point each time, it is shown by the last column of the table that the percentage of difference has more or less the same behavior for every thickness.

Table 3.14: Total Thickness Sensitivity Analysis Results – Case 1

Total Thickness: 6 mm					
Total Thickness	% of Total Thickness	Ply Thickness	External Buckling Pressure [MPa]	Modeshape	%
5.4	-10	0.27	4.66	2.1	-22.1
5.7	-5	0.29	5.52	2.1	-7.8
6	0	0.30	5.99	2.1	0
6.3	5	0.32	7.00	2.1	16.8
6.6	10	0.33	7.55	2.1	26.0
Total Thickness: 8 mm					
Total Thickness	% of Total Thickness	Ply Thickness	External Buckling Pressure [MPa]	Modeshape	%
7.2	-10	0.36	9.35	2.1	-23.5
7.6	-5	0.38	10.69	2.1	-12.5
8	0	0.4	12.22	2.1	0
8.4	5	0.42	13.72	2.1	12.3
8.8	10	0.44	15.42	2.1	26.2
Total Thickness: 10 mm					
Total Thickness	% of Total Thickness	Ply Thickness	External Buckling Pressure [MPa]	Modeshape	%
9	-10	0.45	16.32	2.1	-23.3
9.5	-5	0.475	18.70	2.1	-12.1
10	0	0.5	21.27	2.1	0
10.5	5	0.525	24.06	2.1	13.1
11	10	0.55	27.04	2.1	27.1

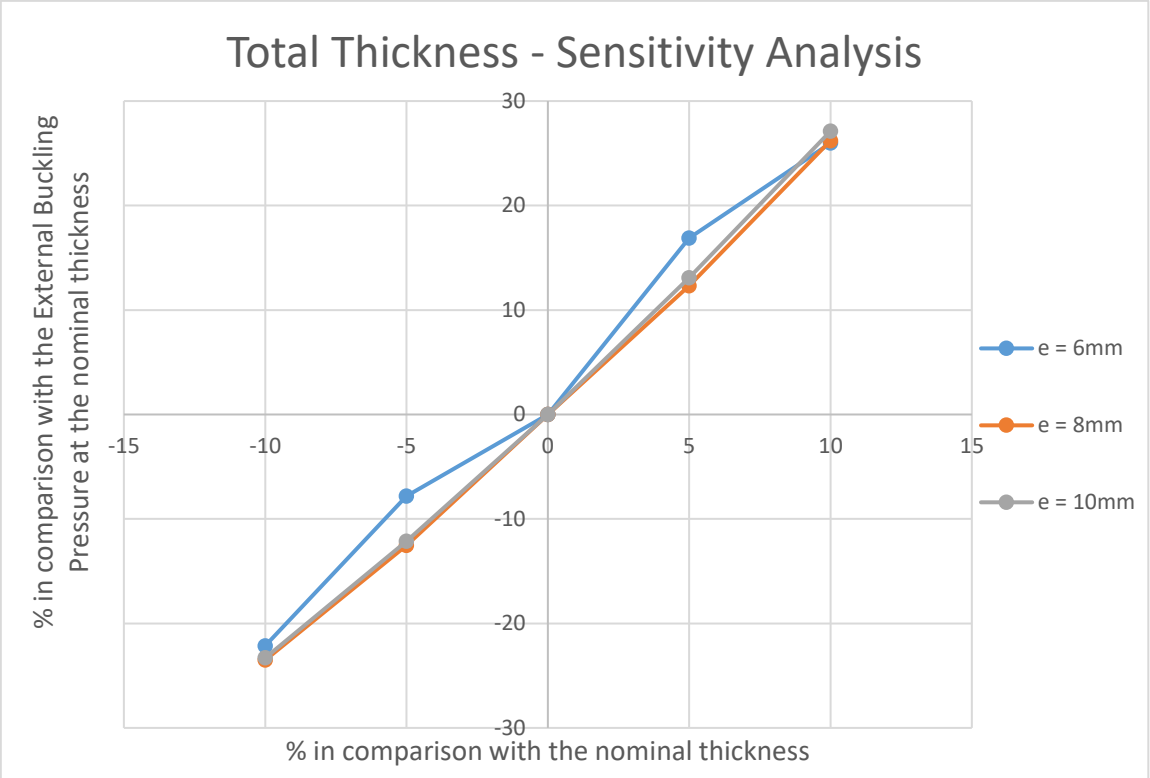

Figure 3.11: Diagram of the Total Thickness Sensitivity Analysis – Case 1

As it is depicted in a more clear way by the diagram in Figure 3.11, the conclusion of this sensitivity analysis is that once the thickness is reduced by 10%, then we can expect an approx. 23% reduction of the buckling pressure. A similar outcome occurs when increasing the thickness by 10%; an approx. 27% increase of the buckling pressure is obtained. It must be underlined that those percentages are considerably high for only 10% increase, which leads to the assumption that the total thickness of the tube will be of great importance for the buckling behavior of the vessel, as expected.

Material Properties

The parameters that remain constant for this study are explained in Table 3.15.

Table 3.15: Constant Parameters – Stacking Sequence Effect.

Total Thickness [mm]	t_{tolal}	8
Ply thickness [mm]	t	1
Number of Plies	n	20
Element Type	S8R	8-node doubly curved thick shell, reduced integration - Structured Quadratic - 6 DOFs
Mesh	-	20 elements circumferentially and 26 longitudinally – 520 elements total
Boundary Conditions	End 1	Fully fixed – All DOFs of all its nodes.
	End 2	Only the Longitudinal Translation is free.
Stacking Sequence	-	$(\pm 55^{o})_{10}$
CFRP	1	Reference Table 3.1

A similar sensitivity analysis has been carried out for the properties of the material as well, the results of which are presented in Table 3.9. Each principal property (E_1, E_2, G_{12}) was decreased and increased by 5 and 10%. Of course, the influence of each principal property on the rest of them was taken into account. For example, it is assumed that E_2 is equal to E_3, this means that for the cases where the E_2 changes, then E_3 is affected in the exact same way. Keeping the nominal property of each case as a reference point each time, it is shown by the last column of the table that the percentage of difference how each property behaves.

Table 3.16: Properties Sensitivity Analysis Results – Case 1

E_1 = 131170 MPa				
E_1	% of E_1	External Buckling Pressure [MPa]	Modeshape	%
118053	-10	11.27	2.1	7.8
124611.5	-5	11.71	2.1	4.2
131170	0	12.22	2.1	0.0
137728.5	5	12.58	2.1	-2.9
144287	10	13.01	2.1	-6.5
$E_2 = E_3$ = 10860 MPa				
E_2	% of E_2	External Buckling Pressure [MPa]	Modeshape	%
9774	-10	12.04	2.1	1.5
10317	-5	12.09	2.1	1.0
10860	0	12.22	2.1	0.0
11403	5	12.20	2.1	0.2
11946	10	12.25	2.1	-0.2
$G_{12} = G_{13} = 2*G_{23}$ = 4160 MPa				
G_{12}	% of G_{12}	External Buckling Pressure [MPa]	Modeshape	%
4149	-10	11.89	2.1	2.7
4379.5	-5	12.02	2.1	1.6
4610	0	12.22	2.1	0.0
4840.5	5	12.26	2.1	-0.4
5071	10	12.38	2.1	-1.3

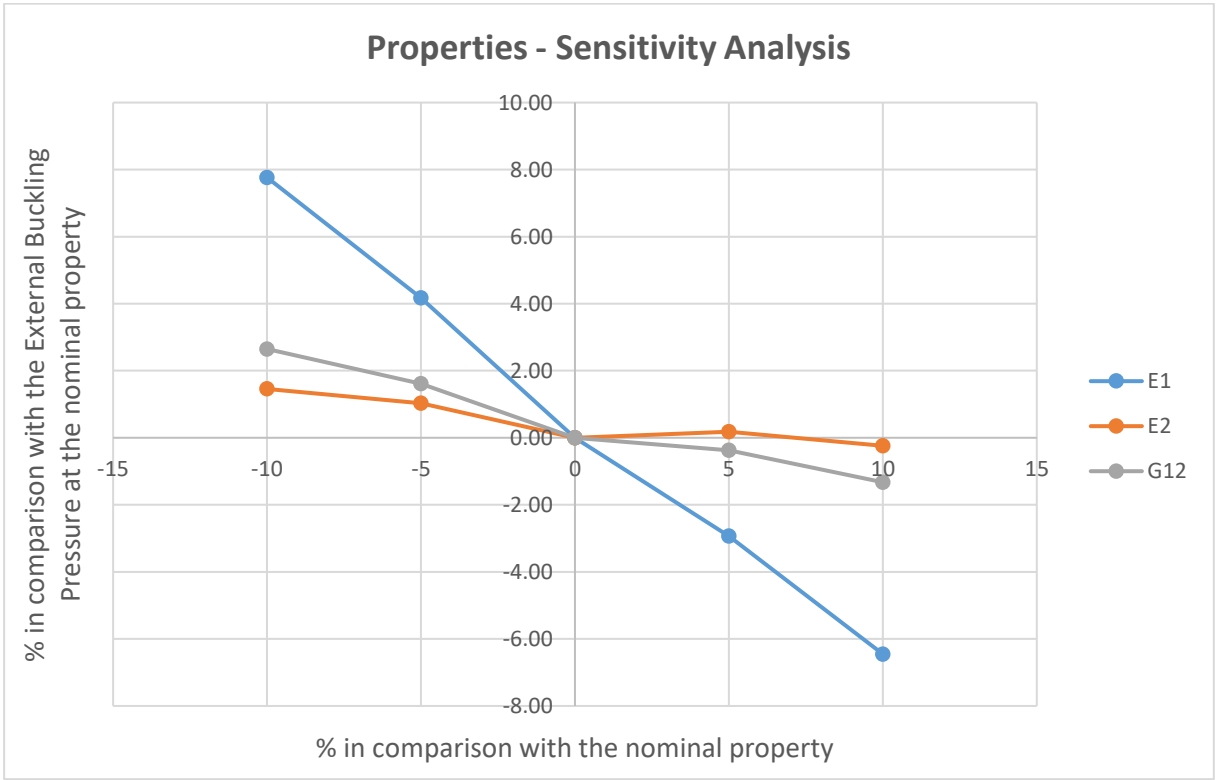

Figure 3.12: Diagram of the Properties Sensitivity Analysis – Case 1

As it is depicted in a more clear way by the diagram in Figure 3.12, it is evident that the most influential factor out of the 3 investigated is the E_1, which represents the longitudinal elastic modulus and it affects the results up to 7,77%. The second most influential is G12 and the third one is E2, but still their influence is very low in comparison with E1.

Ovalization of the Tube

Before examining the optimization of the stacking sequence, which is a very important factor of the study at this point, the effect of the ovalization of the specimen is another factor that has been examined in the context of this sensitivity analysis. The circular shape of the tube changes to an elliptical one by gradual percentages, as shown in Figure 3.13. The buckling results in show that there is failure there. As for the failure of the material, it is observed that failure is detected for percentages higher than 1%, so attention must be drawn there. The results from Table 3.17 are depicted in Figures 3.14 (a) and (b) in the form of diagram.

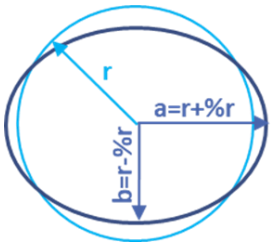

Figure 3.13: Ovalization Explained.

Table 3.17: Buckling and Hashin's results for elliptical variations of the end.

Percentage r%	External Buckling Pressure [MPa]	Hashin's Criterion	
		Fiber	Matrix
0	12.43	0.004	0.001
1	12.43	0.011	0.167
2.5	12.42	0.028	1.098
5	12.41	0.075	4.177

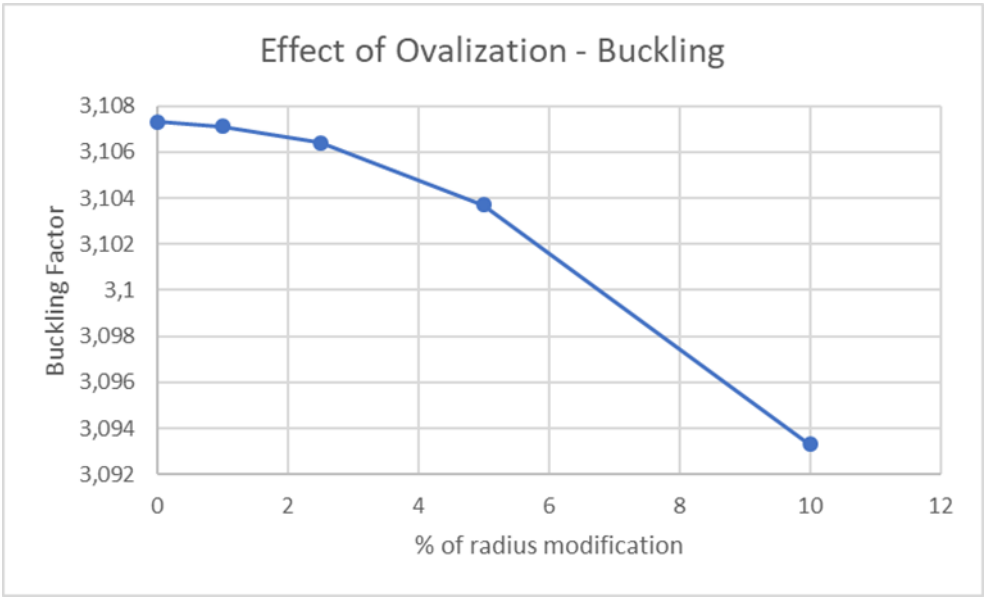

(a)

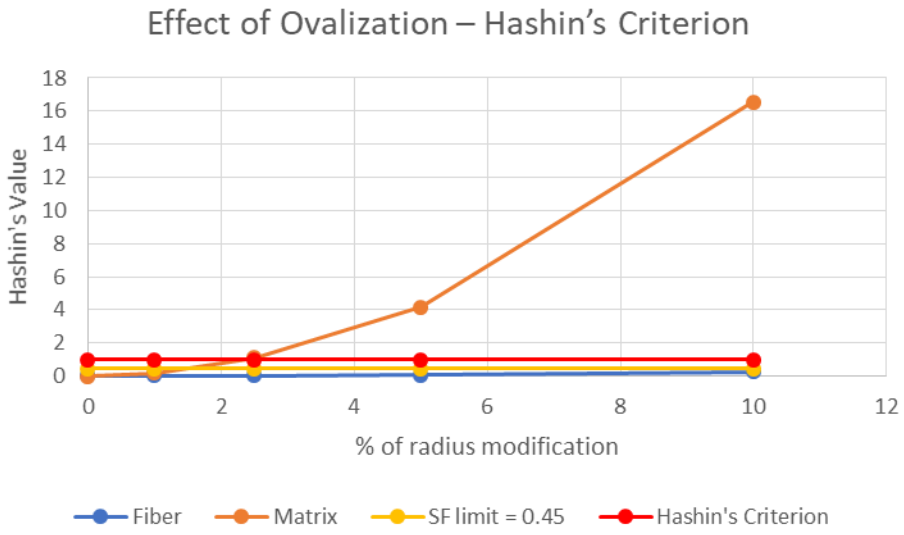

(b)

Figure 3.14: Effect of the Ovalization on the Results of (a) Buckling and (b) Hashin's Criterion.

3.3 Linear Analysis

This means that at the ends of the tube, the boundary conditions are applied to all nodes of a 30 mm wide ring area, representing the part of the tube that is adhesively bonded to the ring of the metal end cup (Figure 3.15). Those new boundary conditions appear in Figure 3.16.

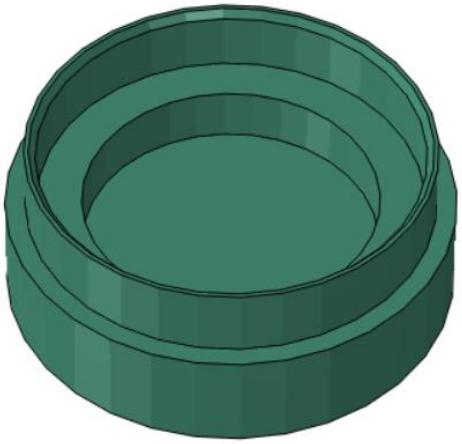

Figure 3.15: Metal End Cup – ABAQUS.

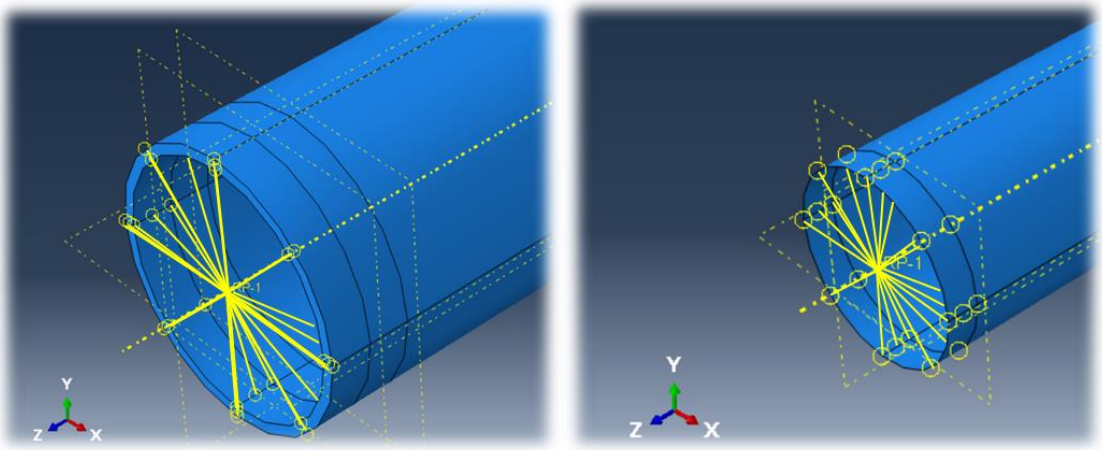

(a) (b)

Figure 3.16: Boundary Conditions – With the Overlap Length for (a) solid elements and (b) shell elements.

A linear analysis is described in the current section, in order to reach a conclusion about the final proposed stacking sequence. Towards this goal, two contradicting requirements must be fulfilled by the same product. The pressure vessel of Case Study 1 must have an adequate stiffness in the circumferential direction, so that it will be able to withstand buckling due to external pressure. On the other hand, the adhesive joint of the end cup requires an increased stiffness in the axial direction of the tube, to avoid high stress concentrations at the end of the 30 mm metal ring protrusion inside the cylinder. This last fact guides to the decision of adding layers on the internal side of the cylinder with fibers as close to the axial direction as possible. As it is mentioned in section 1.4, the filament winding method cannot usually produce plies of 0º, so the winding angle chosen for the axial plies is 15º. In Table 3.18, multiple stacking sequences are examined with solid element models only, with those specific boundary conditions portrayed in Figure 3.16. The ply of interest is Ply 1 because it comes in contact with the adhesive layer. Table 3.18 shows the most stacking sequences with the most promising results, the external buckling pressure they result in and the Hashin's Criterion values they produce for the compression of the fiber and the matrix and the out-of-plane version of the criterion for a node at the mid-length of the cylinder and the end of the adhesion layer respectively.

Table 3.18: Eigenvalue Buckling and Linear Analysis Results – CFRP 1.

SOLID ELEMENTS		Mid-length of Cylinder			End of Adhesion Length		
Stacking Sequence	External Buckling Pressure [MPa]	Fiber	Matrix	Out of Plane	Fiber	Matrix	Out of Plane
$[\pm 55^{o}]_{10}$	12.240	0.027	0.080	0.342	0.955	0.904	1.016
$[\pm 15^{o}]_{1}/[\pm 55^{o}]_{9}$	11.840	0.026	0.137	0.280	0.351	0.506	4.367
$[\pm 15^{o}]_{2}/[\pm 55^{o}]_{8}$	11.280	0.044	0.186	0.201	0.286	0.445	4.852
$[\pm 15^{o}]_{1}/[\pm 55^{o}]_{8}/[\pm 15^{o}]_{1}$	12.360	0.039	0.171	0.398	0.348	0.515	4.905

The values in Table 3.18 result in the conclusion that the cylinder produced based on the assumptions made up until now is not adequate for the applied load, given that some of the examined stacking sequences are failing the safety factor because of the compression of the matrix and all of them fail the Hashin's Criterion because of the out-of-plane value. As a result, this research switches direction from now on when it comes to the properties.

The results for both analyses – eigenvalue and linear – for the CFRP 2 material are displayed in Table 3.19 below.

Table 3.19: Eigenvalue Buckling and Linear Analysis Results – CFRP 2.

SOLID ELEMENTS		Mid-length of Cylinder			End of Adhesion Length		
Stacking Sequence	External Buckling Pressure [MPa]	Fiber	Matrix	Out of Plane	Fiber	Matrix	Out of Plane
$[\pm 55^{o}]_{10}$	11.080	0.002	0.029	0.009	0.051	0.611	0.074
$[\pm 15^{o}]_{1}/[\pm 55^{o}]_{9}$	10.320	0.001	0.060	0.003	0.016	0.108	0.131
$[\pm 15^{o}]_{2}/[\pm 55^{o}]_{8}$	9.840	0.014	0.078	0.002	0.012	0.110	0.176
$[\pm 15^{o}]_{1}/[\pm 55^{o}]_{8}/[\pm 15^{o}]_{1}$	10.080	0.001	0.071	0.005	0.015	0.115	0.153

Fortunately, it is clear that a cylinder made by the CFRP 2 composite produces results that do not exceed the maximum permissible value of the failure criterion. Furthermore, the stacking sequence that seems to be the most appropriate, given the contradicting necessities of Case Study 1 mentioned above, is the $[\pm 15^{o}]_{1}/[\pm 55^{o}]_{9}$. This could be more generalized in the sense that 10% of the total plies of this specific pressure vessel must have a small winding angle.

The results in Table 3.19 show that the value for the compression of the matrix is the governing one calculated by the Hashin's Criterion. That is why in Figure 3.17, its through thickness variation at the mid-length of the cylinder is depicted in the form of diagram for both shell and solid elements. It is evident that after the parametric study, the results of the Hashin's criterion are all lower than the maximum permissible value of the Hashin's Criterion (SF limit), which means that the pressure vessel with the final propositions is perfectly safe for the linear analysis.

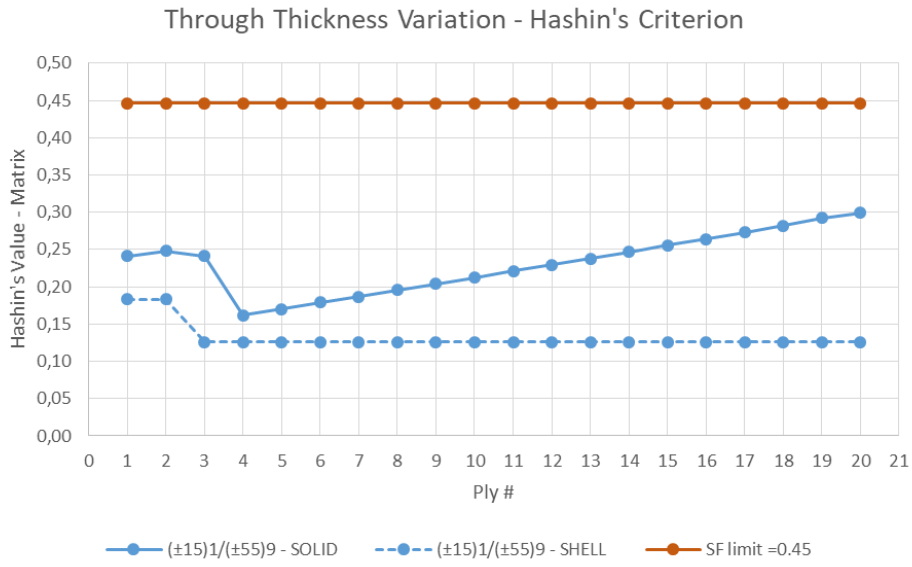

Figure 3.17: Hashin's Matrix Value of every ply.

From this point forward, the material considered is CFRP 2 with a $[\pm 15^{o}]_{1}/[\pm 55^{o}]_{9}$ stacking sequence.

3.4 Nonlinear Buckling Analysis

The linear analyses presented in the previous section can give a general idea of the structure's behavior but they cannot be considered as realistic, taking into account the worst possible deformation scheme of the cylinder, under the action of external pressure. A nonlinear analysis is needed to account for a non-symmetric deformed shape of the cylinder – in other words, a nonlinear finite element analysis is required because the structure is characterized by geometric nonlinearities in real life that affects its behavior greatly. The nonlinear static analysis is an analysis where a nonlinear relation holds between applied forces and displacements. Nonlinear effects can originate from geometrical nonlinearities, material nonlinearities, boundary conditions nonlinearities and contact. The performance of nonlinear static analysis for this case study is chosen in order to examine whether the Hashin's Criterion values of the composite tube change when geometric nonlinearities are taken into account, and in order to take into account initial geometric imperfections of the cylinder. The external pressure is applied incrementally, whereas the internal pressure is applied as constant from the beginning.

The model of Case Study 1 takes into account only geometric nonlinearities. In order to enforce to the cylinder a non-cylindrical deformed shape, an initial geometric imperfection scheme was taken into account. This scheme is identical to the critical buckling modeshape of the cylinder (in this case mode 2.1) and its maximum imperfection with respect to the nominal cylindrical shape was taken equal to either 0.5 or 1% of the nominal external diameter (1 - 2 mm).

The selected settings for the time steps of the nonlinear analysis are displayed in Table 3.18 below.

Table 3.18: Increment Characteristics.

Newton - Raphson	Size of Increments		
No. of Increments	Initial	Minimum	Maximum
40	0.025	0.001	0.025

The objective of this analysis is to have a model that can withstand 100% of the applied load, which is an external pressure of 4 MPa. Table 3.19 presents the key assumptions the model is based on and the values produced by the Hashin's Criterion for the compression of the fiber and the matrix, as well as the region on the cylinder these values are located through the surface and through the thickness. In addition, the safety factor is calculated as the reverse of the Hashin's value for the fibers and matrix respectively. Beginning with the shell elements and a 2 mm max initial imperfection, although the safety factor of the fibers is greater than the required one, the nonlinear calculations for the nominal thickness of 8 mm result to a safety factor for the matrix significantly lower than the required one. Therefore, the model was examined again with a total thickness of 10 mm, in order to enhance its structural behavior. This time, the safety factor for the matrix was higher than the required one, so according to the shell elements, the pressure vessel must be designed with a 25% increased total thickness, in order to obtain an entire composite structure – both fibers and matrix – that can withstand 100% of the applied load.

Table 3.19: Nonlinear Buckling Results for Examined Thicknesses – Shell Elements.

Thickness	8 mm	10 mm
Stacking Sequence	$(\pm15)_1/(\pm55)_9$	$(\pm15)_1/(\pm55)_9$
Initial Imperfection	2 mm	2 mm
Region	Crest	Crest
Ply	3	3
Fiber	0.00725	0.00689
SF - Fiber	137.931	145.138
Ply	1	1
Matrix	0.605	0.375
SF - Matrix	1.65	2.67
S_{11}	-20.786	-16.384
S_{22}	-21.340	-12.904
S_{33}	0.000	0.000
S_{12}	-4.927	-2.377
S_{13}	-	-
S_{23}	-	-

However, this new conclusion must be checked for the solid elements model as well, given that the solid elements calculate also the stresses in the thickness direction (S_{33}, S_{13}, and S_{23}). Similarly, the solid elements models with 1 and 2 mm max initial imperfection provide the results that appear in Table 3.20, which has contents similar to the ones in Table 3.19.

Table 3.20: Nonlinear Buckling Results for Examined Thicknesses – Solid Elements.

Thickness	10 mm	10 mm	12 mm	12mm
Stacking Sequence	$(\pm15)_1/(\pm55)_9$	$(\pm15)_1/(\pm55)_9$	$(\pm15)_1/(\pm55)_9$	$(\pm15)_1/(\pm55)_9$
Initial Imperfection	2 mm	1 mm	2 mm	1 mm
Region	Crest	Crest	Crest	Crest
Ply	3	3	3	3
Fiber	0.0245	0.0458	0.0336	0.0180
SF - Fiber	40.82	21.34	29.76	55.56
Ply	1	1	1	1
Matrix	0.605	0.351	0.374	0.353
SF - Matrix	1.94	2.85	2.67	2.83
S_{11}	2.642	-81.243	21.237	9.968
S_{22}	-15.972	-4.977	-15.570	-11.077
S_{33}	-1.823	-7.801	-1.809	-1.0899
S_{12}	-3.298	0.956	-3.585	-2.517
S_{13}	0.0004	9.670	-0.031	-0.011
S_{23}	0.0015	-2.004	-0.088	-0.035

As it is evident from the calculations above, the safety factor of the fibers is greater than the required one. However, the same cannot be stated for the matrix. Its safety factor is still lower than the required one with a total thickness of 10 mm and an initial imperfection of 2 mm. The matrix does not appear to fail only when the total thickness is increased by 50% in comparison to the nominal one, meaning it becomes equal to 12 mm. Another proposed alternative is to make sure that the initial imperfection will not exceed the 1 mm. This is not impossible as the 2 mm (1 % of the initial diameter) is a large number to assume, hence the worst case scenario.

4. Case Study 2

4.1 Model Description

4.1.1 Geometry

The initial geometry of the tube is internal diameter equal to 450 mm and external one to 503 mm, resulting to a nominal thickness of 26.5 mm. The cylinder lengths that will be examined are 500, 1250 and 2000 mm. The domes are hemispherical and they have the same internal and external diameter as the cylindrical part.

This case study has the particularity that in reality, the domes are filament wound. One of the main parameters of the design of a composite filament wound pressure vessel is the winding angle of the fibers. The winding angle is the angle between the fiber path and the longitudinal axis of the cylinder (for cylindrical shapes) [Peters et al., 2011]. Another concern relatively to the filament winding method is the composite layers' variable winding angles and thicknesses, while approaching the top of the domes. In that hemispherical area, the winding angle reduces itself gradually while approaching the top of the domes to an almost axial direction (0º) and the thickness of the layer increases due to the significant overlapping of numerous bands. It must be taken into account that the thickness of the composite material and the winding angle of the fibers influence the structural behavior of the vessel. This means that the domes must be modeled in a way, so that the winding angle and thickness variation can participate in the calculation of the results. One often-used method for dealing with such a problem is partitioning the domes of the model into "slices" and assigning thickness and winding angle values to each one separately [Azeem et al., 2022]. That is the process followed for the domes of the modeled pressure vessel, whose slices are depicted in Figure 4.1.

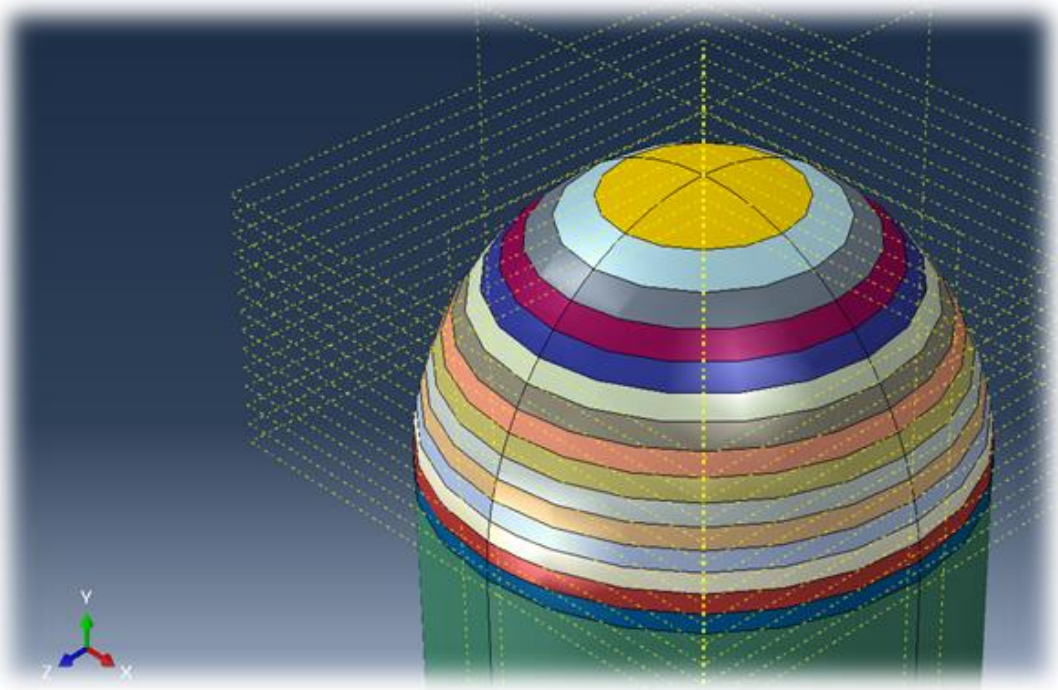

Figure 4.1: The slices on the domes.

It must be mentioned that in this thesis, only the winding angle is a variable parameter throughout the slices while approaching the top of the dome. After all, the domes are modeled

mostly for providing their stiffness to the cylinder's ends and the modeling of slices is a great approximation either way.

The slices are identical in terms of area [mm^2] and are numbered in a wat where the first one is right after the cylindrical part and the last one is at the top of the dome. As for the winging angle variation starting from the end of the cylindrical part and reaching the pole at the top of the domes, the sequence used to determine the angle at the boundary of each slice with the next one is the following:

$$\theta_z = \theta_{z-1} - \left(\frac{\theta_1}{z_{total}}\right) \qquad (4-1)$$

z = {1,2, …, z_{total}}: the number of each boundary

$z_{total} = \{5, 10, 15\}$: the total number of the boundary

θ_z : the winding angle of the z boundary

θ_1 : the winding angle of the cylindrical part

In order for the function of equation (4-1) to be clearer, the following example is provided. Assuming that the total number of slices is equal to 15 ($z_{total} = 15$), the winding angle of the cylindrical part is equal to 55º ($\theta_1 = 55$), then the winding angle of the boundary between the first and the second slice (z = 2) is equal to:

$$\theta_2 = \theta_1 - \left(\frac{\theta_1}{z_{total}}\right) = 55 - \frac{55}{15} = 51.33^0 \qquad (4-2)$$

For the boundary between the second and third slice (z = 3) is equal to:

$$\theta_3 = \theta_2 - \left(\frac{\theta_1}{z_{total}}\right) = 51.33 - \frac{55}{15} = 47.67^0 \qquad (4-3)$$

And so on.

The final winding angle with which the entire slice is modeled is the average of the angles respective to the boundaries that surround it. This means that, following the example above, the winding angle of the first slice is equal to:

$$\theta_{1,2} = \frac{\theta_1 + \theta_2}{2} = 53.17^0 \qquad (4-4)$$

The winding angle of the second slice is equal to:

$$\theta_{2,3} = \frac{\theta_2 + \theta_3}{2} = 49.50^0 \qquad (4-4)$$

And so on.

4.1.2 Material

The type of material for the pressure vessels is CFRP, so the options came down to the type of carbon fibers and resin. The composite material that was finally opted for (CFRP 2, 24K

fibers and a bisphenol A type of epoxy), the properties of which are derived from Moon's et al. (2010). The properties of both CFRP candidates are reminded in Table 4.1 below. For the sake of completeness, results for both materials will be presented.

Table 4.1: Material Properties of candidate CFRPs

CFRP		**CFRP 1**	**CFRP 2**	-
	Fiber	12K T700	24K T700	-
	Matrix	Epoxy	Bisphenol A	-
Elastic modulus	E_1	131.17	121.00	GPa
	E_2	10.86	8.60	GPa
	E_3	10.86	8.60	GPa
Poisson's ratio	v_{12}	0.280	0.253	-
	v_{13}	0.280	0.253	-
	v_{23}	0.382	0.421	-
Shear modulus	G_{12}	4.61	3.35	GPa
	G_{13}	4.61	3.35	GPa
	G_{23}	2.31	2.68	GPa
Tensile strength	X_T	1060.93	2060.00	MPa
	Y_T	26.08	32.00	MPa
	Z_T	26.08	32.00	MPa
Shear strength	S_{12}	9.23	45.00	MPa
	S_{13}	9.23	45.00	MPa
	S_{23}	4.62	64.00	MPa

4.1.3 Stacking Sequence

Due to the fact that the material is a filament wound composite, the stacking sequence will be formed in pairs. The initial stacking sequence that the tube is modeled with is 5 pairs of ±55º $[(\pm 55^{\circ})_5]$, adding up to 10 plies, 2.65 mm thick each. The reason behind choosing the 55º as the initial winding angle is because it is concluded after multiple researches that it is the optimum winding angle by the first ply failure approach of filament wound composite tubes [Tsouvalis et al. (2000), Martins et al. (2014), Almeida et al. (2017)].

Furthermore, the plies of the stacking sequence are layered from the inside to the outside of the cylinder, meaning that Ply 1 is located internally all the way to Ply 10, which is located externally.

4.1.4 Types of Elements & Mesh

This case study has been modeled with shell elements only. The types of elements chosen are 8-node shell elements with 6 degrees of freedom. The mesh is structured quadratic and the nodes are placed in such a way, so that the elements' aspect ratio is equal to 1 for the cylindrical part, resulting in mostly square shaped elements. [Tsouvalis et al., 2000].

More specifically, the initial mesh applied to the cylinder is 94 elements circumferentially and 34 longitudinally, and then for each slice the mesh magnitude differed with the aim to keep the aspect ratio of the elements almost equal to 1. Figure 4.2 (a) presents the types of elements chosen for the models and (b) the initial mesh of the model.

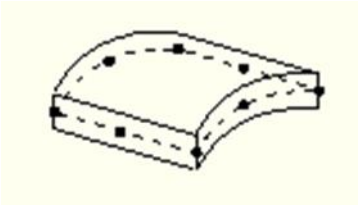

S8R

(a)

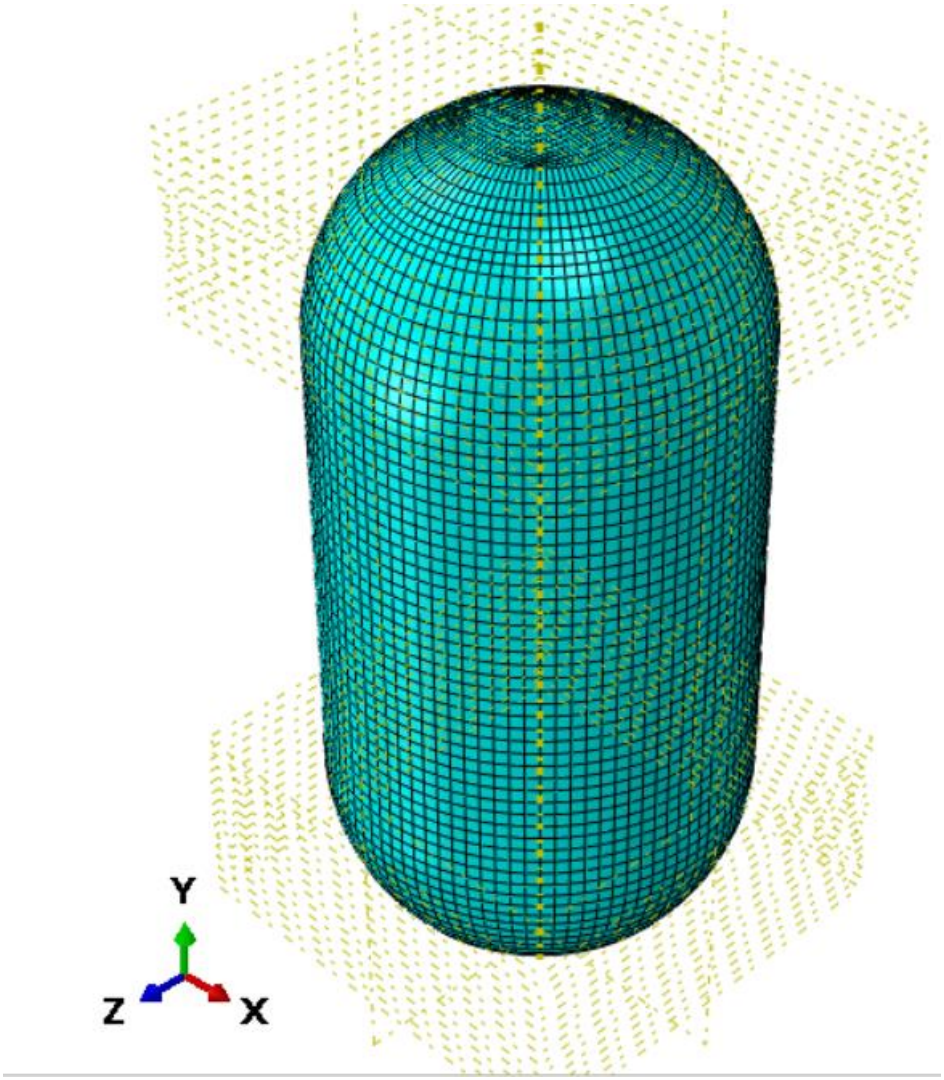

(b)

Figure 4.2: (a) S8R elements used by ABAQUS. (b) Mesh of Case Study 2 - Shell Elements.

4.1.5 Boundary Conditions & Loads.

The initial boundary conditions that are proposed are visible in Figure 4.2.

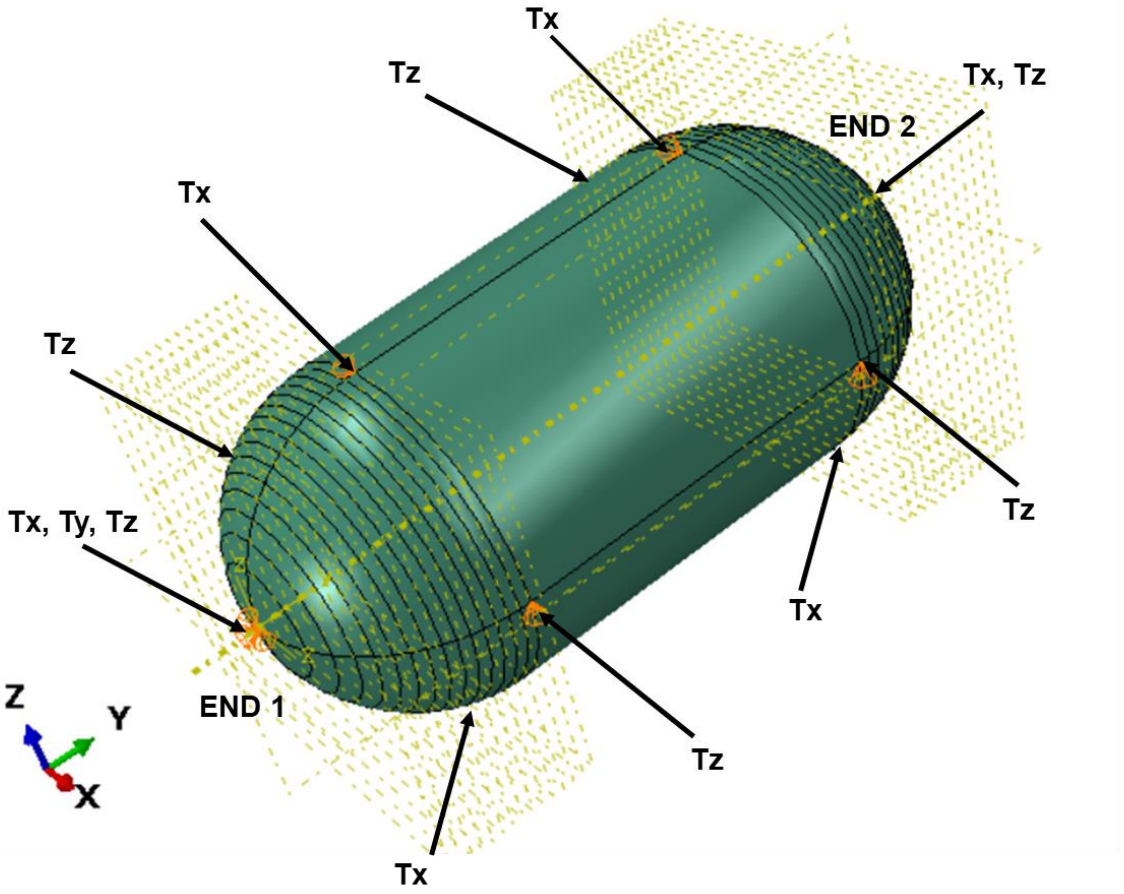

Figure 4.3: Boundary Conditions for Case Study 2.

For End 1, the pole at the top of the dome is pinned (all translations Tx, Ty and Tz are fixed). For End 2, the pole at the top of the dome has its transverse translations fixed only (Tx and Tz). Furthermore, in order to avoid any rigid body rotation with respect to the cylinder axis, which is not expected to happen in real life anyway, on each interface of the tube with the domes there are 4 points equally distributed at 90 deg circumferentially that have their circumferential translation fixed [Tsouvalis et al, 2000].

For load case 1, the loads applied on this tube are 5 MPa externally and 0.1 MPa internally and for load case 2, there are 0.1 MPa external pressure and 27.5 MPa internal.

4.2 Linear Analysis & Parametric Studies

Similarly to case study 1, this research continues with a parametric study based on the linear analysis, in order to start settling on the final characteristics of the composite tube. The conducted analysis is linear and not buckling, because the governing load case for this pressure vessel is load case 2, where the internal pressure is higher. This means that no buckling occurs. The goal is to model the structure in the most realistic way that is possible and to optimize it to the point that the loads applied can be withstood by the pressure vessel. The parameters examined in these next sections are:

1. Number of Slices on the Domes
2. Mesh Convergence Study

3. Total Thickness Effect
4. Stacking Sequence Effect & Number of Plies
5. Effect of Boundary Conditions

The parametric study was done based on the model with the length of 500 mm and the results in this section are calculated based on the material properties of CFRP 2, given that it has already been chosen for case study 1 and the two cases are to be manufactured with the same material.

4.2.1 Number of Slices on the Domes

The total number of slices examined for the domes of this case are 5, 10 and 15. Table 4.2 shows the results obtained from each model, which include the values of the Hashin's Criterion for the tension of the fiber and the matrix. Those values are calculated at the first ply, at the nodes appearing in Figure 4.4, whose Y-coordinate and position on the pressure vessel, which are also included in Table 4.2. It is only fair to choose the model with the highest number of slices for accuracy purposes, however, it is interesting to observe that by adding more slices, the pressure vessels becomes stiffer.

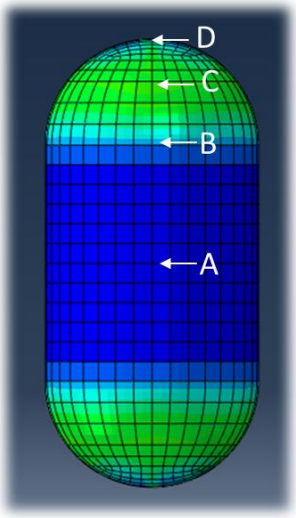

Figure 4.4: Nodes where the results have been calculated

Table 4.2: Number of Slices Effect – Results – Case 2.

5 Slices		Ply 1		
Y - Coordinate	Position	Fiber	Matrix	Failure
A - 475	Mid-length	0.0278	0.0574	no
B - 725	Interface	0.0749	0.1101	no
C - 884	Dome	0.1066	0.4482	Yes
D - 950	Pole	0.9568	17.0301	YES
10 Slices		Ply 1		
Y - Coordinate	Position	Fiber	Matrix	Failure
A - 475	Mid-length	0.0279	0.0576	no
B - 725	Interface	0.0169	0.0704	no
C - 884	Dome	0.1071	0.4229	no
D - 950	Pole	2.6201	25.5306	YES
15 Slices		Ply 1		
Y - Coordinate	Position	Fiber	Matrix	Failure
A - 475	Mid-length	0.0279	0.0648	no
B - 725	Interface	0.0604	0.0816	no
C - 884	Dome	0.1945	0.5325	Yes
D - 950	Pole	2.3878	15.3718	YES

4.2.2 Mesh Convergence Study

The first step of the parametric study concerns the meshing of the model. The parameters that remain constant for this study are explained in Table 4.3.

Table 4.3: Constant Parameters – Mesh Convergence Study.

Total Thickness [mm]	t_{tolal}	26.5
Ply thickness [mm]	t	2.65
Total plies	n	10
Element Type	S8R	8-node doubly curved thick shell, reduced integration - Structured Quadratic - 6 DOFs
Boundary Conditions	-	Reference Figure 4.3
Number of Slices	-	15
CFRP	2	Reference Table 4.1
Stacking Sequence	-	$(\pm 55^{o})_5$
Load Case 1 [MPa]	P_{ext}	0.1
	P_{int}	27.5

The final mesh to be chosen must be the least fine, so that the computational time will be as short as possible but without influencing the accuracy of the results. The mesh magnitude is following the same process as the previous section – the aspect ratio is kept as close to being equal to 1 as possible. Table 4.4 demonstrates the various number of elements examined, their aspect ratio, the highest displacements the respective model calculates and the percentage of difference each respective displacement presents in comparison to the one calculated by the model with the least fine mesh. Moreover, Figure 4.4 depicts those results in a form of a diagram.

Table 4.4: Mesh Convergence Study – Displacements – Case 2.

Elements	Aspect Ratio	U_1 [mm]	U_2 [mm]	U_3 [mm]	% of U_1	% of U_2	% of U_3
Mid-length of the cylinder					% in comparison with the U at the least fine meshing		
7964	1.03	-0.121	0.351	0.000	0.000	0.000	0.000
18408	1.09	-0.122	0.352	0.000	0.575	0.306	0.000
70000	1.00	-0.122	0.353	0.000	0.362	0.656	0.012
At the interface of the domes with the cylinder					% in comparison with the U at the least fine meshing		
7964	1.30	-0.110	0.289	0.000	0.000	0.000	0.000
18408	1.30	-0.111	0.290	0.000	0.898	0.348	0.000
70000	1.25	-0.111	0.291	0.000	0.707	0.788	0.000
On the domes					% in comparison with the U at the least fine meshing		
7964	1.12	-0.217	0.294	-0.004	0.000	0.000	0.000
18408	1.03	-0.220	0.294	-0.004	1.265	-0.050	-12.500
70000	1.05	-0.219	0.296	-0.003	0.932	0.518	-22.500

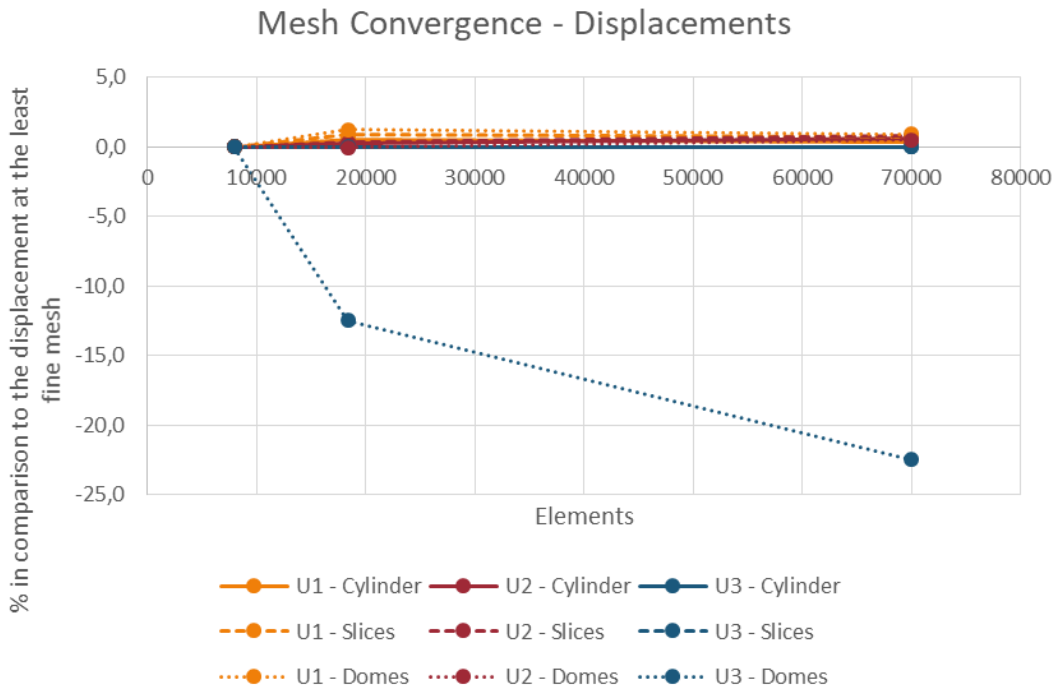

Figure 4.4: Diagram of the Mesh Convergence Study – Displacements - Case 2.

The same procedure was followed for the stresses, so as to observe their convergence as well. Table 4.5 demonstrates the various number of elements examined, their aspect ratio, the highest stresses the respective model calculates and the percentage of difference each respective stress presents in comparison to the one calculated by the model with the least fine mesh. Moreover, Figure 4.5 depicts those results in a form of a diagram.

Table 4.5: Mesh Convergence Study – Stresses – Case 2.

Elements	Aspect Ratio	S_1 [mm]	S_2 [mm]	S_3 [mm]	% of S_1	% of S_2	% of S_3
Mid-length of the cylinder					% in comparison with the S at the least fine meshing		
7964	1.03	-57.988	-4.725	-1.458	0.000	0.000	0.000
18408	1.09	-57.952	-4.722	-1.455	-0.062	-0.067	-0.199
70000	1.00	-57.980	-4.722	-1.456	-0.014	-0.058	-0.145
At the interface of the domes with the cylinder					% in comparison with the S at the least fine meshing		
7964	1.300	-62.876	-7.085	-0.486	0.000	0.000	0.000
18408	1.300	-62.289	-7.148	-0.526	-0.934	0.882	8.228
70000	1.250	-63.103	-7.084	-0.546	0.362	-0.024	12.282
On the domes					% in comparison with the S at the least fine meshing		
7964	1.120	7.800	-14.556	-4.076	0.000	0.000	0.000
18408	1.030	5.768	-14.547	-4.002	-26.056	-0.058	-1.801
70000	1.050	5.731	-14.582	-3.917	-26.524	0.179	-3.905

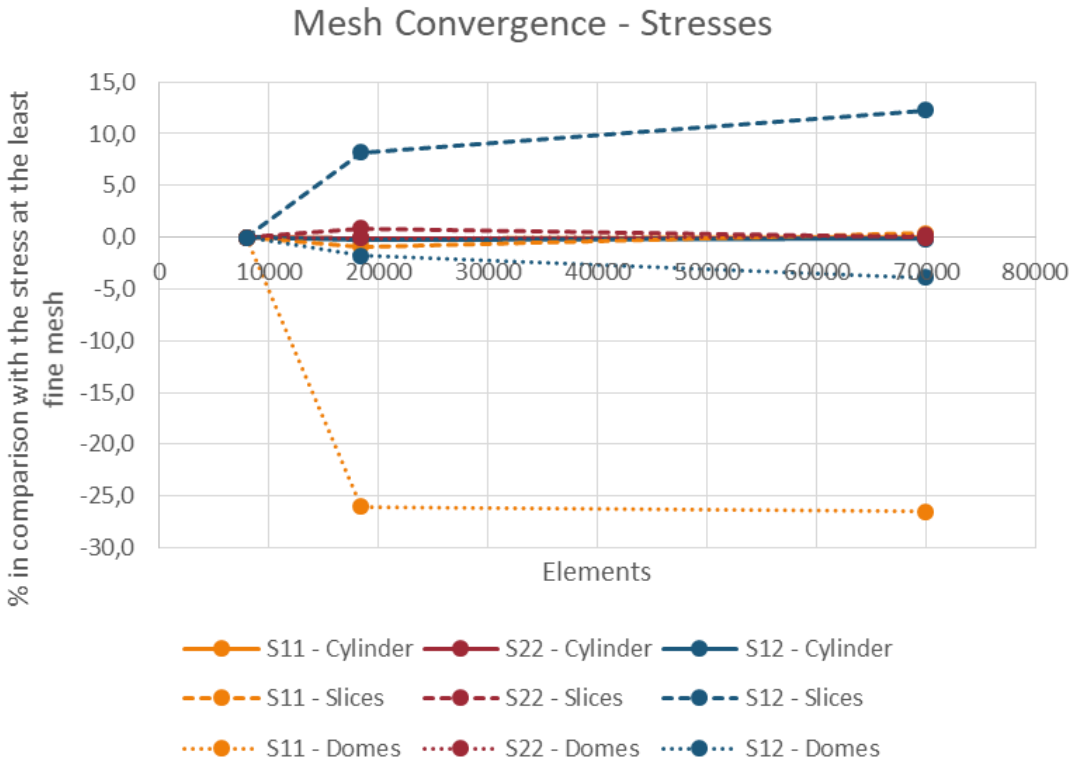

Figure 4.5: Diagram of the Mesh Convergence Study – Stresses – Case 2.

Based on the displayed results above, it is obvious that the model was more or less converged from the beginning, apart from the domes, which is normal because there are stress concentrations and important approximations. Nevertheless, this does not affect the fact that the least fine mesh can be chosen once again, given that at the end of the day the domes are modeled for providing their stiffness to the cylinder's ends. This means that a total of 7964 elements – for the cylindrical part: 94 circumferentially and 34 longitudinally with an aspect ratio of 1.03 – are a safe choice for this model.

4.2.3 Total Thickness Effect

At this point of the research, the issue that must be tackled is the fact that with the given assumptions, the pressure vessel fails. That is why the total thickness is up for examination straight away. The parameters that remain constant for this study are explained in Table 4.6.

Table 4.6: Constant Parameters – Total Thickness Effect.

Total plies	n	10
Element Type	S8R	8-node doubly curved thick shell, reduced integration - Structured Quadratic - 6 DOFs
Boundary Conditions	-	Reference Figure 4.3
Number of Slices	-	15
CFRP	2	Reference Table 4.1
Stacking Sequence	-	$(\pm 55^{o})_5$
Mesh	-	7964 in total - 96x34 for the cylinder
Load Case 1 [MPa]	P_{ext}	0.1
	P_{int}	27.5

The aim once again is to obtain a model that calculates a matrix value lower than the maximum permissible value of the Hashin's Criterion (SF limit = 0.45). From Figure 4.6, it is clear that in order to achieve that, the total thickness must be increased by 10 mm, meaning that the final proposed thickness is 37.7% higher than the initial one and it ends up equal to 36.5 mm. Also, from Figures 4.7 and 4.8, it is obvious that the pressure vessel's behavior stays the same as its length increases. Another information that can be obtained from this step is that the thickness of an individual ply is equal to 3.65 mm, since there are 10 equally thick plies.

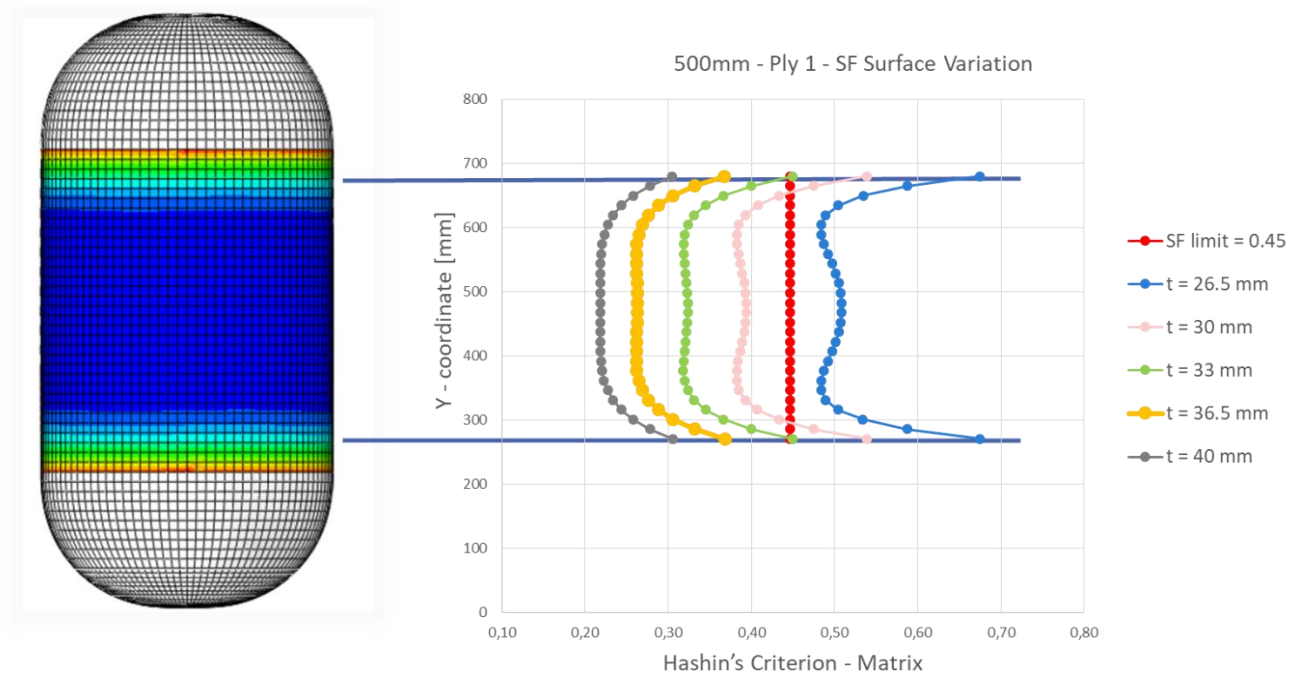

(a) (b)

Figure 4.6: (a) Max Hashin's Value Surface Variation (b) Diagram of the SF for Various Thicknesses – Internal Pressure – 500 mm.

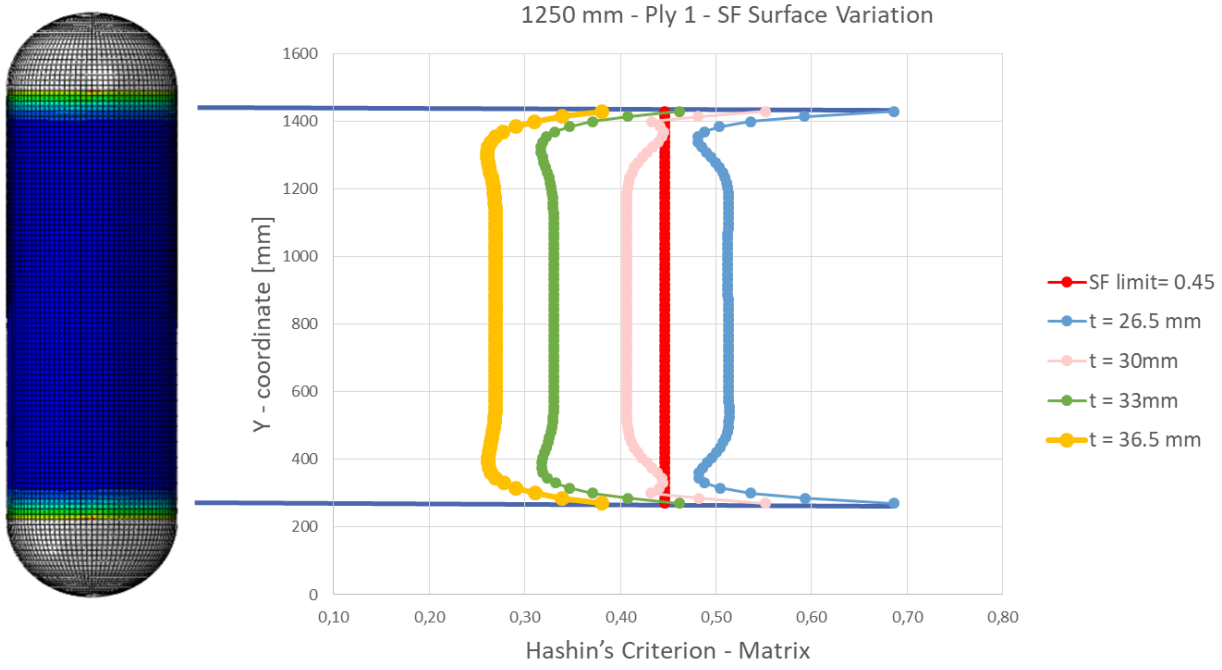

(a) (b)

Figure 4.7: (a) Max Hashin's Value Surface Variation (b) Diagram of the SF for Various Thicknesses – Internal Pressure – 1250 mm.

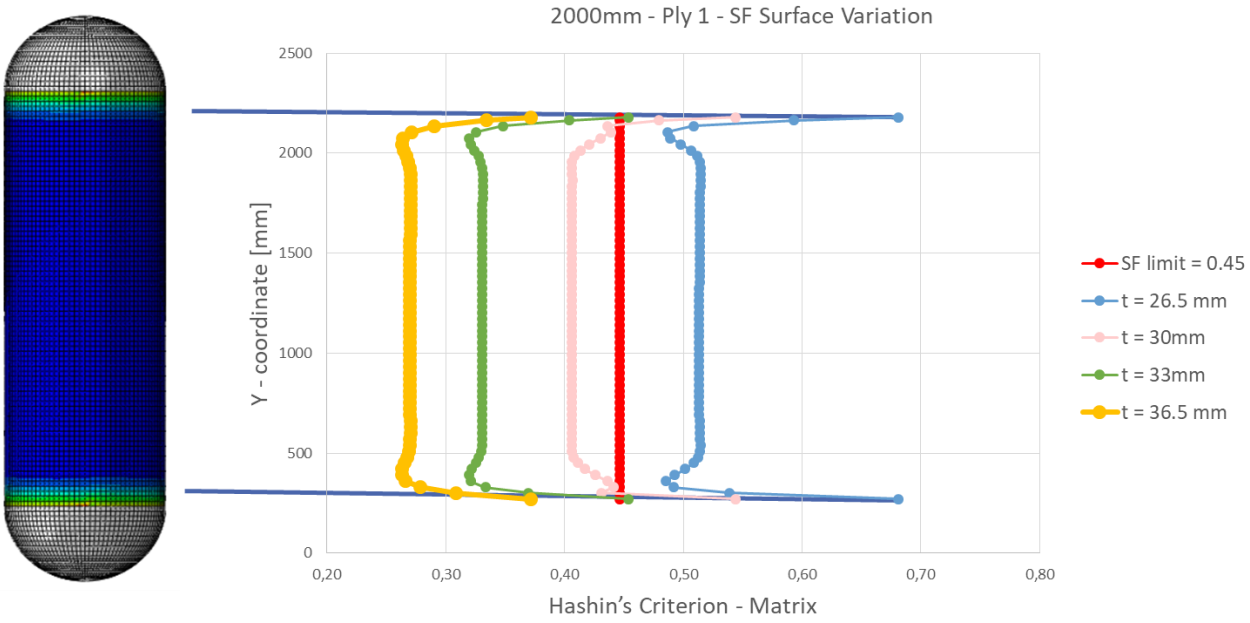

(a) (b)

Figure 4.8: (a) Max Hashin's Value Surface Variation (b) Diagram of the SF for Various Thicknesses – Internal Pressure – 2000 mm.

4.2.4 Stacking Sequence Effect

This next part examines the stacking sequence effect on the behavior of the tube. The parameters that remain constant for this study are explained in Table 4.7.

Table 4.7: Constant Parameters – Stacking Sequence Effect.

Element Type	S8R	8-node doubly curved thick shell, reduced integration - Structured Quadratic - 6 DOFs
Total plies	n	10
Total Thickness [mm]	t_{tolal}	36.5
Ply thickness [mm]	t	3.65
Boundary Conditions	-	Reference Figure 4.3
Number of Slices	-	15
CFRP	2	Reference Table 4.1
Mesh	-	7964 in total - 96x34 for the cylinder
Load Case 1 [MPa]	P_{ext}	0.1
	P_{int}	27.5

Table 4.8 demonstrates the various stacking sequences examined, the values at the mid-length of the cylinder for the tension of the fiber and the matrix, based on the Hashin's Criterion and the plies where those values are located, for the fibers and the matrix respectively. Moreover, Figure 4.9 depicts those results in a form of a diagram.

Table 4.8: Stacking Sequence Effect – Hashin's Criterion – Case 1.

Stacking Sequence [±θº]	Fiber	Ply	Matrix	Ply	Difference to $[\pm 55^º]_5$ [%]
$[\pm 55^º]_5$	0.013	1	0.281	10	0.00
$[\pm 45^º]_5$	0.012	1	1.340	10	376.87
$[\pm 60^º]_5$	0.012	1	0.904	1	221.71
$[\pm 15^º]_1/[\pm 55^º]_4$	0.019	3	0.288	10	2.49
$[\pm 55^º]_4/[\pm 15^º]_1$	0.019	8	0.802	10	185.41
$[\pm 15^º]_1/[\pm 55^º]_3/[\pm 15^º]_1$	0.030	3	1.248	10	344.13
$[\pm 55^º]_4/[\pm 87^º]_1$	0.014	1	0.723	10	157.30
$[\pm 87^º]_1/[\pm 55^º]_4$	0.014	3	0.719	1	155.87

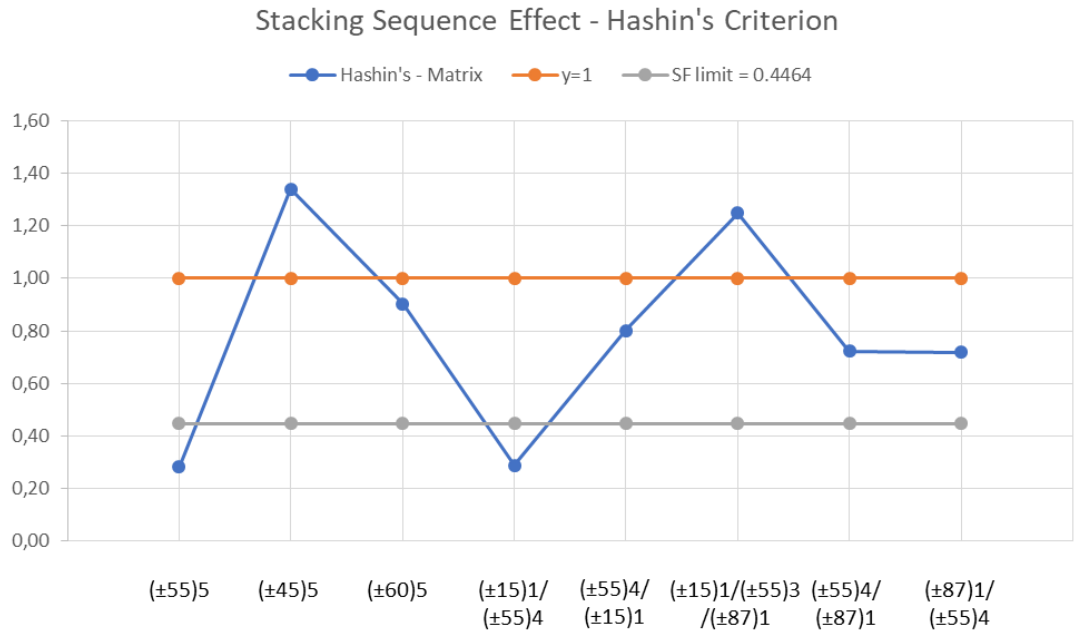

Figure 4.9: Diagram of the Stacking Sequence Effect – Case 2.

As one can easily predict, the higher Hashin's Criterion value – hence, the governing one – is respective to the matrix. From Figure 4.9, it seems that the maximum permissible value if the failure criterion (SF limit) is exceeded for every examined stacking sequence apart from the $[\pm 55^{o}]_{5}$ and the $[\pm 15^{o}]_{1}/[\pm 55^{o}]_{4}$. However, the initial stacking sequence seems to have the lowest matrix value. It is important to note that the stacking sequence is a parameter that is able to affect the results up to almost 377%. It must be mentioned that the model has been tested with a doubled amount of plies (20 plies – 10 pairs) and the results on the cylindrical part, which this thesis focuses on, show that the difference caused by doubling the layers was not higher than 7%, as seen in Table 4.9, which shows the values of the Hashin's Criterion for the tension of the fiber and the matrix at the first ply, both for 10 plies and for 20 plies. The nodes, where those results are calculated appear in Figure 4.10, whose Y-coordinate and position on the pressure vessel are also included in Table 4.9.

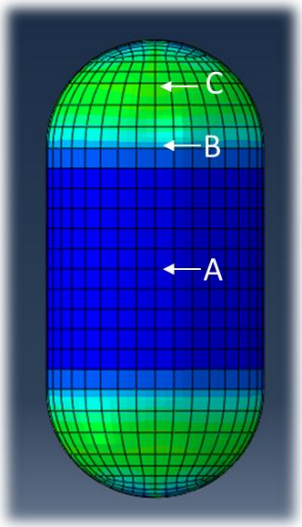

Figure 4.10 : Nodes where the results have been calculated.

Table 4.9: Number of Plies Effect – Results – Case 2.

5 Pairs – 10 Plies		Ply 1		
Y - Coordinate	Position	Fiber	Matrix	Failure
A - 475	Mid-length	0.013	0.264	no
B - 725	Interface	0.016	0.531	no
C - 884	Dome	0.000	2.430	YES
10 Pairs – 20 Plies		Ply 1		
Y - Coordinate	Position	Fiber	Matrix	Failure
A - 475	Mid-length	0.013	0.264	no
B - 725	Interface	0.016	0.568	no
C - 884	Dome	0.000	2.410	YES

This means that the proposed stacking sequence remains the initially proposed one: $[\pm 55^{o}]_5$.

4.2.5 Effect of Boundary Conditions

At this point, the boundary conditions are up for examination. The relative movement between the node right at the mid-length of the cylindrical part and the node right on top of the dome is the difference between the displacements of those exact nodes and it is presented in Table 4.10 for each load case. The various sets of boundary conditions (BC) are presented in Table 4.10 as well in the form of "BC of End 1 / BC of End 2 / BC for 4 points equally distributed around the interfaces of the cylindrical part with the domes". The differences calculated amongst the various sets of boundary conditions were none.

Table 4.10: Candidate Sets of Boundary Conditions – Case 2.

LOAD CASE 1	Longitudinal Translation (U3)		
Boundary Conditions	Mid-length of Cylinder	Pole at the Top of the Dome	Relative Movement
Pinned/U1,U3	0.385	0.769	0.3845
Pinned,R2/U1,U3,R2	0.385	0.769	0.3845
U1,U3,R3	0.010	0.395	0.3846
Pinned/U1,U3/X/Z	0.385	0.769	0.3846
LOAD CASE 2	Longitudinal Translation (U3)		
Boundary Conditions	Mid-length of Cylinder	Pole at the Top of the Dome	Relative Movement
Pinned/U1,U3	-2.151	-4.301	-2.1505
Pinned,R2/U1,U3,R2	-2.151	-4.301	-2.1505
U1,U3,R3	-0.056	-2.207	-2.1505
Pinned/U1,U3/X/Z	-2.151	-4.301	-2.1505

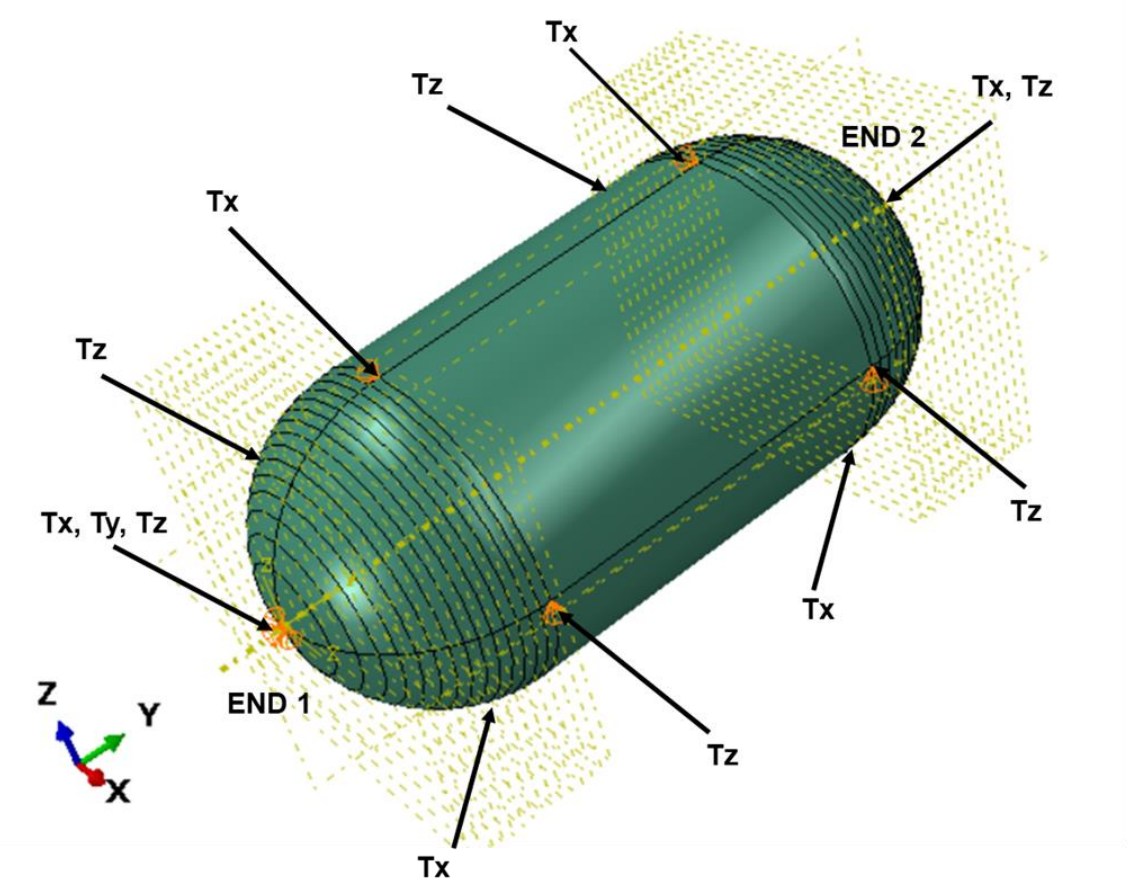

Figure 4.11: Boundary Conditions for Case Study 2.

So, the chosen set is displayed in Figure 4.11 and it is the same as the proposed one: End 1 is pinned on the top of the dome, End 2 has the transverse translations on the top of the dome fixed and additionally on each interface of the domes with the cylindrical part 4 points equally distributed around the perimeter have their circumferential translations fixed [Tsouvalis et al, 2000].

4.3 Nonlinear Analysis

The linear analysis explained in the previous sections can give a general idea of the structure's behavior but often a linear analysis is not considered realistic enough. A nonlinear analysis is needed, since there is a nonlinear relationship between the forces and the subsequent displacements of the pressure vessel – in other words, a nonlinear finite element analysis is required because the material is characterized by geometric nonlinearity in real life that affects its behavior greatly.

It must be mentioned that there are two types of nonlinearities related to Case Study 2: material and geometric nonlinearities, however, the finite element environment of ABAQUS has a function only for the geometric ones. Furthermore, in this case, the governing loading case is one with higher pressure internally. As a result, there is no buckling during the analysis and there is no initial imperfection introduced to the model based on some modeshape – like it was

for Case Study 1. This fact leads to the expectation that the nonlinear analysis will not calculate results that are greatly different to the ones provided by the linear analysis.

The method used for the nonlinear analysis is the Newton – Raphson Method. The characteristics of the increments are displayed in Table 4.8 below.

Table 4.8: Increment Characteristics.

Newton - Raphson	Size of Increments		
No. of Increments	Initial	Minimum	Maximum
40	0.025	0.001	0.025

The analysis was carried out for each one of the 3 lengths and the results were compared with the ones from the linear analysis. The difference of the average matrix value based on the Hashin's Criterion through the cylinder's surface between Linear and Nonlinear for each length is shown by the following percentages:

- 0.83% for 500 mm.
- 4.85% for 1250 mm.
- 1.32% for 2000 mm.

This means that the average difference overall is that the results of the Hashin's Criterion of the nonlinear analysis are 2.33% lower than those derived from the linear one. This percentage is considerably low and it allows this research to reach the conclusion that the linear analysis is enough for Case Study 2.

4.4 Final Results

Based on all the analyses and studies performed above, the final results were calculated and are displayed in the following tables and the deformed shape for each analysis is depicted in the respective figures. The deformation scale in the pictures is equal to 50.

Table 4.9: Eigenvalue Buckling Results – Load Case 1.

Length [mm]	Buckling Factor	External Buckling Pressure [MPa]	Mode shape	No. of Elements	Cylinder's Mesh
500	13.62	68.11	2.1	7964	96x34
1250	10.13	50.65	2.1	18408	96x84
2000	9.43	47.14	2.1	70000	96x136

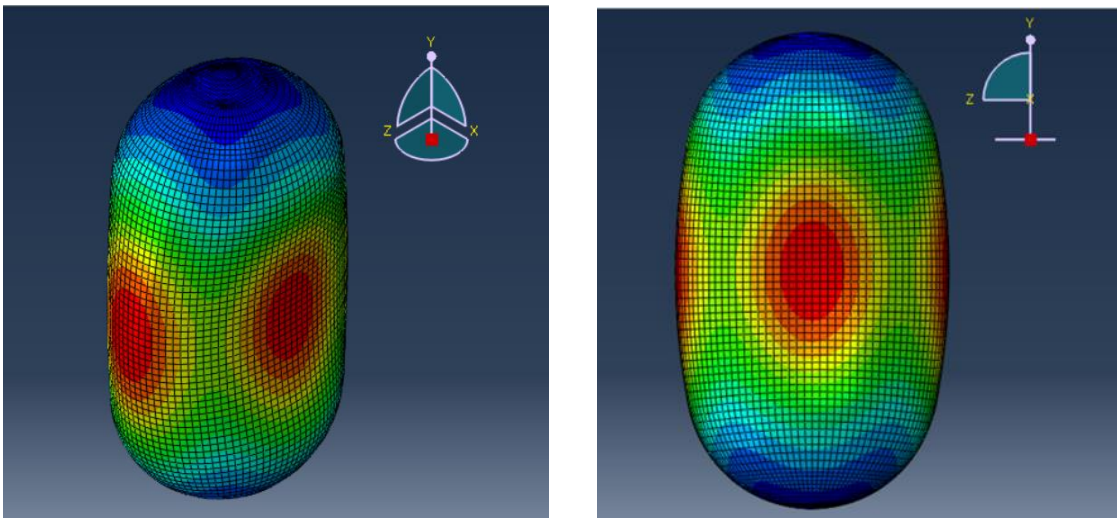

(a) (b)

Figure 4.12: Buckling Modeshape resulting from Load Case 1 – 500 mm.

Table 4.10: Linear Analysis Results – Load Case 1.

Length [mm]	Fiber	Safety Factor	# Ply	Y-Coordinate [mm]	Matrix	Safety Factor	# Ply	Y-Coordinate [mm]
500	0.001	1000	1	680	0.096	10.42	1	680
1250	0.001	1000	1	1430	0.096	10.42	1	1430
2000	0.001	1000	1	2180	0.097	10.41	1	2180

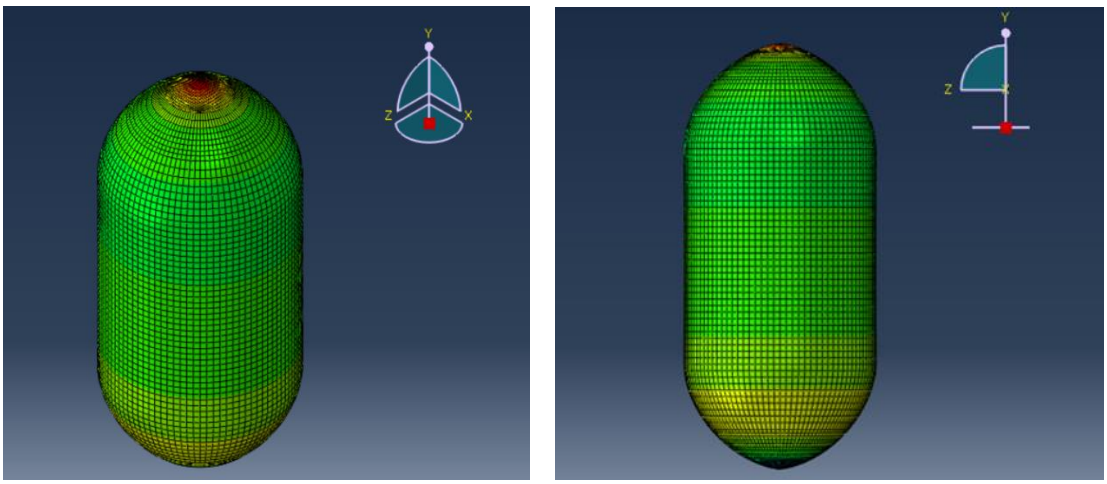

(a) (b)

Figure 4.13: Deformation resulting from Load Case 2 – 500 mm.

Table 4.11: Linear Analysis Results – Load Case 2.

Length [mm]	Fiber	Safety Factor	# Ply	Y-Coordinate [mm]	Matrix	Safety Factor	# Ply	Y-Coordinate [mm]
500	0.014	71.43	1	680	0.368	2.72	1	680
1250	0.014	71.43	1	1430	0.369	2.71	1	1430
2000	0.014	71.43	1	2180	0.371	2.70	1	2180

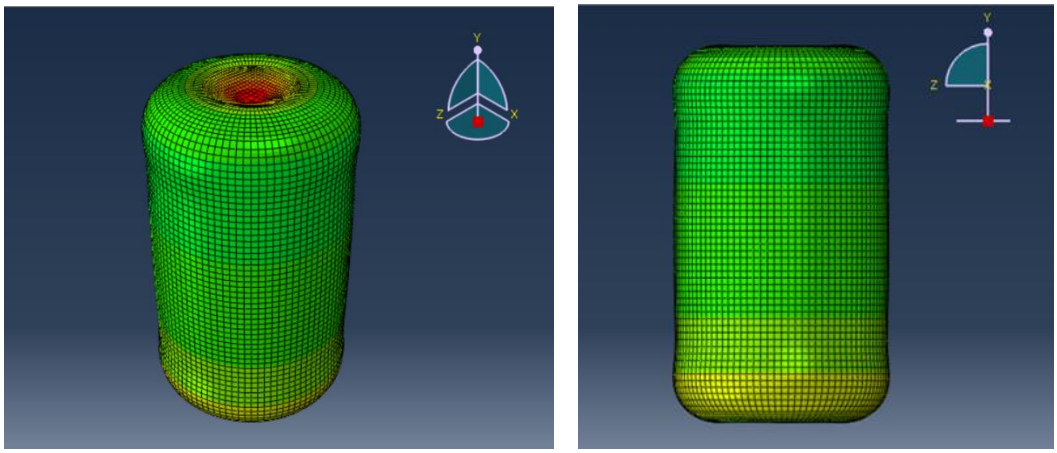

(a) (b)

Figure 4.14: Deformation resulting from Load Case 2 – 500 mm.

5. Conclusions

5.1 Case Study 1

5.1.1 *Conclusive remarks*

The parametric study performed in this case study results in various conclusions regarding the characteristics of the cylinder. Firstly, based mostly on the eigenvalue buckling analysis, the parameters that have been examined can be ranked as follows, based on the difference they cause to the buckling pressure:

1. Stacking Sequence. (Differences up to 60%)
2. Cylinder Thickness. (Differences up to 27%)
3. Boundary Conditions. (Differences up to 20%)
4. Material Properties. (Differences up to 7.77%)
5. Number of Plies. (Differences up to 3.14%)
6. Mesh Magnitude. (Differences up to 0.033%)

Furthermore, certain changes must be made to the initial modeling assumptions, which affect the final actual product as well. More specifically, the cylinder with the initially proposed stacking sequence ($[\pm 55^{o}]_{10}$) and made by the CFRP 1 composite, results in matrix and out-of-plane Hashin criteria values higher than the maximum permissible one. That is why the material changes to CFRP 2 (24K T700 – epoxy Bisphenol A), which has similar elastic and shear moduli, but has higher tensile strength parallel and perpendicular to the fibers and higher shear strength.

After switching material properties, the issue to be tackled is the demand for two contradicting requirements that must be fulfilled by the same product. The pressure vessel must have an adequate stiffness in the circumferential direction, so that it will be able to withstand buckling due to external pressure and at the same time, it must have increased stiffness in the axial direction, so that high stress concentrations will be avoided at the end of the 30 mm metal ring protrusion inside the cylinder. This guides to the decision of replacing the first pair of the stacking sequence with one pair of $[\pm 15^{o}]$. This means that the final proposed stacking sequence is $[(\pm 15^{o})_1/(\pm 55^{o})_9]$. Adding more pairs of 15º-plies resulted in lower ability to withstand buckling. This could be more generalized in the sense that 10% of the total plies of this specific pressure vessel must have a small winding angle.

Finally, the model underwent a nonlinear analysis, which resulted in Hashin's Criterion values lower than the maximum permissible one for the fibers, but higher for the matrix. As a result, the nominal thickness is considered a moderate option, since the fibers are deemed safe. However, this thesis provides a more conservative option, where both the fibers and the matrix are 100% not failing even with an initial imperfection equal to 1% of the nominal external diameter. This solution is increasing the total thickness by 50%, resulting in a total thickness of 12 mm, keeping the external diameter constant.

5.1.2 Comparison with a parallel study focused on the joint with the metal end cup

As it has been mentioned several times in this thesis, a parallel research was performed at the same time as this one, which was focused on the adhesive joint and the metal end cup. This

research calculated the same type of results but by a more detailed model, which included the adhesive layer, the metal ring and the metal end cup. In fact, that is why the set of boundary conditions used in section 3.3 include the 30 mm metal ring protrusion inside the cylinder – in order to have a similar model to that research, but focused on the composite cylinder. The conclusions derived from that parallel research are the same to the present ones, in a qualitative way. More specifically, the cylinder with the initially proposed stacking sequence ($[\pm 55^{o}]_{10}$) and made by the CFRP 1 composite results in matrix and out-of-plane values higher than the maximum permissible one of the Hashin's Criterion and the governing value for the nonlinear analysis is the matrix value. In addition, the Hashin's Criterion values were lower than the maximum permissible one for the fibers, but higher for the matrix. The matrix values of the two studies present the following differences:

- For a total thickness of 8 mm and an initial imperfection of 2 mm, the difference was 4%. However, the present study calculated results only for shell elements. The parallel study used solid elements.
- For a total thickness of 12 mm and an initial imperfection of 2 mm, the difference was 11%. The types of elements are the same; both studies used solid elements.
- For a total thickness of 12 mm and an initial imperfection of 1 mm, the difference was 16%. The types of elements are the same; both studies used solid elements.

A point of difference between the two studies is the location of the predicted matrix failure in the case of the thicker cylinder. According to the parallel study, the higher value of the Hashin's Criterion of the matrix is situated in the adhesive joint end, however, in this thesis, the higher corresponding values are situated in the mid-length crest, since the details of the adhesive joint are not modelled at all.

5.1.3 Future Research

When it comes to the future of research for this case study, there are many ways to proceed. It is important to emphasize the fact that the material properties introduced to the model are based on the literature. So, the next proposed step is to produce specimens representative of the pressure vessel in geometry, so that experiments can be carried out and the actual mechanical properties of the proposed material can be determined. After that, the design and the characteristics of the pressure vessel will be adapted to those actual material properties.

5.1 Case Study 2

5.2.1 Conclusive remarks

The parametric study performed in this case study for the 500 mm long cylindrical part results in various conclusions regarding the characteristics of the pressure vessel. Firstly, based on the linear static analysis and with load case 2 applied, the parameters that have been examined can be ranked as follows, based on the difference they cause to the strength load of the vessel:

1. Stacking Sequence. (Differences up to 377%)
2. Total Thickness. (Differences up to 57%)
3. Number of Slices. (Differences up to 12.9 %)

4. Number of Plies. (Differences up to 7%)
5. Mesh Magnitude. (Differences up to 0.9 %)
6. Boundary Conditions. (Differences up to 0%)

Furthermore, certain changes must be made to the initial modeling assumptions, which affect the final actual product as well. More specifically, the cylinder with the initially proposed stacking sequence ($[\pm 55^{o}]_{10}$) and made by the CFRP 1 composite results in matrix Hashin criterion values higher than the maximum permissible one. That is why the material changes to CFRP 2 (24K T700 – epoxy Bisphenol A), which has similar elastic and shear moduli but has higher tensile strengths parallel and perpendicular to the fibers and higher shear strength.

After switching mechanical properties, the results of the cylindrical part keep indicating failure, which means that another parameter must change. The total thickness is the most effective change to be made, in order to influence positively the results. And it looks like, just like in case study 1, there is a moderate option of choosing the nominal thickness and relying on the fibers, which seem to not fail. However, the matrix values of the Hashin's Criterion indicate that the matrix exceeds the required safety margin set by the safety factor for the material failure. This leads to the conservative option of increasing the total thickness to 36.5 mm (37.7% increase), keeping the internal diameter constant, so that the entire cylinder does not fail.

Finally, the model underwent a nonlinear analysis, which resulted in Hashin's Criterion values reduced by 2.33% in comparison to the ones derived from the linear static analysis.

5.2.2 Future Research

The next step proposed for this case study concerns the more accurate modeling of the domes. For instance, the thickness variation of the material on the domes is a parameter that's overlooked in this study. It would be beneficial for the accuracy of the results to introduce it to the numerical model in a realistic way. As a matter of fact, there are extensive tools in ABAQUS that can help with modelling a filament wound composite material. Incorporating them to the process could provide information on whether the current way of modeling the domes is adequate or not. It is also proposed to create a model with solid elements, in order to determine the out-of-plane version of the Hashin's Criterion as well and see if they affect the results at all.

6. References

ABAQUS Analysis User's Manual

ANSYS Analysis User's Manual

Agarwal, B. D., & Broutman, L. J. (1990). Composites, *Analysis and Performance of Fiber*. Jonh Wiley & Sons, Inc.

Almeida, J. H. S., Ribeiro, M. L., Tita, V., & Amico, S. C. (2017). Stacking sequence optimization in composite tubes under internal pressure based on genetic algorithm accounting for progressive damage. *Composite Structures*, *178*, 20–26. https://doi.org/10.1016/j.compstruct.2017.07.054

Azeem, M., Ya, H. H., Alam, M. A., Kumar, M., Stabla, P., Smolnicki, M., Gemi, L., Khan, R., Ahmed, T., Ma, Q., Sadique, M. R., Mokhtar, A. A., & Mustapha, M. (2022). Application of Filament Winding Technology in Composite Pressure Vessels and Challenges: A Review. *Journal of Energy Storage, 49*, 103468. https://doi.org/10.1016/j.est.2021.103468

BV NR 546 (2021), Hull in Composite Materials and Plywood, Material Approval, Design Principles, Construction and Survey.

Chatzinas, A. (2021). Experimental parametric study of mechanical properties measurement of filament wound composites and application of statistical analysis. Diploma Thesis. School of Naval Architecture and Marine Engineering, National Technical University of Athens.

Cohen, D. (1997). Influence of filament winding parameters on composite vessel quality and strength. *Composites Part A-Applied Science and Manufacturing*, *28*(12), 1035–1047. https://doi.org/10.1016/s1359-835x(97)00073-0

Davies, P. (2016). Behavior of marine composite materials under Deep Submergence. *Marine Applications of Advanced Fibre-Reinforced Composites*, 125–145. https://doi.org/10.1016/b978-1-78242-250-1.00006-5

Galletly, G.D., James, S., Kruzelecki, J. & Pemsing, K.(1987), *Interactive buckling tests on cylinders subjected to external pressure and axial compression*, Trans. ASME, 109, 10–18.

Geier, B., Meyer-Piening, H., & Zimmermann, R. (2002). On the influence of laminate stacking on buckling of composite cylindrical shells subjected to axial compression. *Composite Structures*, *55*(4), 467–474. https://doi.org/10.1016/s0263-8223(01)00175-1

Martins, L., Bastian, F., & Netto, T. (2014). Reviewing some design issues for filament wound composite tubes. *Materials &Amp; Design*, *55*, 242–249. https://doi.org/10.1016/j.matdes.2013.09.059

Moon, C. J., Kim, I. H., Choi, B. H., Kweon, J. H., & Choi, J. H. (2010). Buckling of filament-wound composite cylinders subjected to hydrostatic pressure for underwater vehicle applications. *Composite Structures*, *92*(9), 2241–2251. https://doi.org/10.1016/j.compstruct.2009.08.005

Mouritz, A. P., Gellert, E., Burchill, P., & Challis, K. (2001). Review of Advanced Composite Structures for naval ships and submarines. *Composite Structures*, *53*(1), 21–42. https://doi.org/10.1016/s0263-8223(00)00175-6

Razavi Setvati, M., Mustaffa, Z., Shafiq, N., & Syed, Z. I. (2014). A review on composite materials for offshore structures. *Volume 5: Materials Technology; Petroleum Technology*. https://doi.org/10.1115/omae2014-23542

Ross, C.T.F., (2011) *Pressure vessels. External pressure technology.* Second edition

Rubino, F., Nisticò, A., Tucci, F., & Carlone, P. (2020). Marine application of fiber reinforced composites: A Review. *Journal of Marine Science and Engineering*, *8*(1), 26. https://doi.org/10.3390/jmse8010026

Papadakis A.Z., Konstantinidis, G. K., Tsouvalis N.G. (2018), Long Term Sea Exposure Effect on the Mechanical Properties of Filament Wound Composites, in Proceedings of the ECCM18 18th European Conference on Composite Materials (ECCM18), 24-28th June 2018, Athens, Greece.

Papadakis A.Z., Tsouvalis N.G. (2016), An Experimental and Numerical Study of CFRP Pressure Housings for Deep Sea Environment Research, in Proceedings of the 26th International Ocean and Polar Engineering Conference (ISOPE-2016), Rhodes, Greece.

Peters, S. T., Green, J., Koussios, S., Priestley, A. P., Lowrey McLarty, J., Leslie, J. & Reynolds, H. (2011). *Composite Filament Winding*.

Tsonos, A. (2021). Structural Design of CNG Storing Composite Pressure Vessels for Marine Applications. Diploma Thesis. School of Naval Architecture and Marine Engineering, National Technical University of Athens.

Tsouvalis, N. G., (1998). *Analysis and Design of Vessels from Composite Materials.* Course Notes. School of Naval Architecture and Marine Engineering, National Technical University of Athens.

Tsouvalis, N. G., Zafeiratou, A., & Papazoglou, V. (2000). Parametric Study of Composite Cylinders Under Hydrostatic Load: Effect of End Closures and Lay-up. IASS-IACM 2000, Chania-Crete, Greece